K-MATRIX FITS TO $\pi N \to N\pi$ AND $N\pi\pi$ IN THE RESONANCE REGION $\sqrt{s}$ = 1.3 TO 2.0 GeV

Table of Contents

K-MATRIX FITS TO $\pi N \to N\pi$ AND $N\pi\pi$ IN THE RESONANCE REGION $\sqrt{s}$ = 1.3 TO 2.0 GeV

Ronald S. Longacre †

Lawrence Berkeley Laboratory
University of California
Berkeley, California 94720

October 1973

ABSTRACT

Starting with partial wave amplitudes for $\pi N \to N\pi$ and $\pi N \to$ several isobar model states of $N\pi\pi$, we are able to apply the constraint of unitarity (using the K-matrix). This permits the removal of the overall phase ambiguity of the isobar amplitudes at each energy. The K-matrix fits generated a smooth prescription for the T-matrix amplitudes, enabling us to search the complex energy plane for poles. The uniqueness of these poles was demonstrated by doing Breit-Wigner refits to the fitted T-matrix amplitudes. The success of the refits and the obvious interpretation justified a simple determination of coupling signs for which there can be checks with theory. This thesis corresponds closely to a forthcoming paper submitted to Physical Review except that here the K-matrix is based on a 1972 solution "A" isobar-model fits to $N\pi\pi$ data, and in the final paper we use solution "B."

†Present address: D. Ph. P. E., CEN Saclay, 91 Gif-Sur-Yvette, France.

1. INTRODUCTION

1.1 Recently partial wave amplitudes in the context of the isobar model have become available for the reaction $\pi N \to N\pi\pi$.[1] Here we present the results of a K-matrix fit to both these amplitudes and the elastic amplitudes,[2,3] $\pi N \to \pi N$. In addition we extract from the amplitudes of the K-matrix fit resonance parameters (mass, widths, couplings, poles).

$N\pi\pi$ partial wave analysis[1] spans the center-of-mass (c.m.) energy range $1300 < E < 2000$ MeV, except for a 100-MeV gap $1540 < E < 1650$ MeV, where the data are not yet available to us. We utilize the data in the most efficient manner, making simultaneous maximum likelihood fits[4] to the three major channels at each energy:

$$\pi^- p \to \pi^+ \pi^- n,$$

$$\pi^- p \to \pi^- \pi^0 p,$$

$$\pi^- p \to \pi^+ \pi^0 p .$$

The inelastic partial wave cross sections we obtain are in excellent agreement with the predictions from elastic phase shift analyses (EPSA).[2,3]

The isobar final states that we have specifically considered are

$$\pi N \to \pi\Delta$$

$$\to \rho_s N$$

$$\to \epsilon N.$$

The subscript s refers to the spin of the ρN system ($s = 1/2$ or $3/2$), referred to as ρ_1 or ρ_3. Since between the energies 1.3 to 2.0 GeV $N\pi\pi$ is the most important inelastic reaction, it is fruitful to use unitarity to describe both elastic and inelastic processes together. For this purpose a coupled channel K-matrix equation was used. We assumed one could describe the resonant states as poles in the K-matrix and

then fit for the pole position and residues. Where the data indicated the need for large additional contributions, we added the appropriate poles, thus providing additional evidence for poorly established resonance states.

Another motivation for doing the K-matrix fits was to determine the one overall phase at each energy of the isobar amplitudes. Once this phase is determined, Argand diagrams are then possible and we can establish the relative signs of the couplings for different channels and resonances from resonance region to resonance region.

Finally the problem of determing reliable resonance parameters from the amplitudes of the K-matrix fit is discussed. Several different ways of estimating resonance parameters, notably the widths, are considered.

1.2 Relation between this thesis and a forthcoming paper: This thesis is the same as the Physical Review paper except for input isobar amplitudes, some tables, and appendices. The input isobar amplitudes for this thesis come from unpublished LBL/SLAC partial wave analysis references.[1,4,5]

2. K-MATRIX FORMALISM

In this section we will discuss how three-particle cross sections can be described in terms of the isobar model amplitudes. We also discuss how an integral K-matrix equation can be reduced to an algebratic equation. Furthermore we introduce the parametrization of our K-matrix which is used to describe simultaneously $N\pi \to N\pi$ and $N\pi\pi \to N\pi\pi$ partial wave amplitudes.

The cross section for $2 \to 3$ particle processes in our normalization is

$$\sigma = \frac{(2\pi)^4}{4F}\int |T_{23}|^2 \delta^4(P-\Sigma_i q_i)\frac{1}{(2\pi)^9}\frac{d^3\vec{q}_1}{2e_1}\frac{d^2\vec{q}_2}{2e_2}\frac{d^3\vec{q}_3}{2e_3}, \quad (1)$$

where P is overall four-momentum and q_i is the four-momentum of the ith particle in the final state:

$$q_i = (e_i, \vec{q}_i). \quad (2)$$

F is the Møller invariant flux factor:

$$F = |Q_1|\sqrt{s}\,. \quad (3)$$

Here Q_1 is the c.m. momentum of the beam particle and $\sqrt{s}$ is the c.m. energy of the system. Finally T_{23} is the invariant matrix element for the $2 \to 3$ particle process.

We are interested in the cross section of an incoming angular momentum state and want to use the isobar model amplitudes determined in Ref. 1. We follow the notation of Ref. 1. The three-particle final state has four independent variables at each value of s. Let us choose them to be two diparticle masses (squared) (s_n and s_m) and two angles (θ and ϕ). We will denote these variables as a vector $\vec{\omega}$. We then assume $T_{23}(\vec{\omega})$ to be a sum of contributions from isobar partial wave amplitudes,

$$T_{23}(\vec{\omega}) = \sum_k t_k(\vec{\omega}), \quad (4)$$

where the subscripts include both isobars (Δ, ρ, ϵ) and partial wave (J^P) indices. For details see Ref. 5. Inserting this partial wave decomposition into Eq. (1) and integrating over the angles θ, ϕ, we find

$$\sigma = \frac{\pi}{4Q_1\sqrt{s}}\sum_J (J+1/2)\left[\sum_n \int |T^J_{1n}(s_n, s)|^2 \frac{Q_n q_n ds_n}{4\sqrt{s}\,4\sqrt{s_n}}\right.$$

$$\left. + \sum_n \sum_{m\neq n} \iint T^{J*}_{1n}(s_n, s)\,\Phi^J_{nm}\,T^J_{1m}(s_m, s)\,ds_n\,ds_m\right], \quad (5)$$

where n is the value of k which is fed by a single incoming wave J, Q_1 is the beam momentum, Q_n the isobar momentum, and q_n the momentum of the isobar decay products. (Q_1, Q_n are in the center of mass, but q_n is evaluated in the isobar rest frame). Finally the ϕ^J_{nm} are the usual recoupling coefficients (Ref. 6 and Appendix C in Ref. 13). We have completely changed the subscripts and introduced the following notation: T^J_{in} represents the partial wave amplitude from the Nπ state (labeled i) to a final state n, formed by an isobar (the nth isobar) and remaining particle. Notice that we have not yet integrated over the diparticle mass (Dalitz plot) s_n, s_m.

We now introduce a K-matrix representation for T. Graves Morris[7] has shown that given an amplitude $T_{if}(p_{i_\alpha}, q_{f_\beta})$, where i is the incoming state of up to three particles ($\alpha \leq 3$), f is the outgoing state of up to three particles ($\beta \leq 3$), and p, q are the four-momenta of the particles, one can write a function $K_{if}(p_{i_\alpha}, q_{f_\beta})$ which is free from all two particle cuts and is related to $T_{if}(p_{i_\alpha}, q_{f_\beta})$ by an integral equation.

$$T_{if}(p_{i_\alpha}, q_{f_\beta}) - K_{if}(p_{i_\alpha}, q_{f_\beta}) = \frac{i}{2}\sum_{m'} \int_{k=1}^{\sigma} \frac{d^3\vec{P}_k}{2\epsilon_k} T_{im'}(p_{i_\alpha}, P_{m'_\sigma}) \times K_{m'f}(P_{m'_\sigma}, q_{f_\beta}) \delta^4(P - \sum_j^\sigma P_j) . \quad (6)$$

If $K_{if}(p_{i_\alpha}, q_{f_\beta})$ is Hermitian then $T_{if}(p_{i_\alpha}, q_{f_\beta})$ is unitary. [This is shown from Eq. (13)]. If we expand T_{if} in a partial wave decomposition as we did above, we obtain (γ = two-body; j, k = three-body states; i → several n isobar; and f → several m isobar for a given J^P state)

$$T^J_{nm} - K^J_{nm} = \frac{i}{2}\sum_\gamma T^J_{n\gamma} \frac{Q_\gamma}{4\sqrt{s}} K^J_{\gamma m} + \frac{i}{2}\sum_j \int \frac{T^J_{nj} Q_j q_j K^J_{jm}}{4\sqrt{s}\ 4\sqrt{s_j}} ds_j + \frac{i}{2}\sum_j \sum_{k \neq j} \int T^J_{nj} \Phi^J_{jk} K^J_{km} ds_j ds_k .$$

If we include the stable two-body states and also the diagonal elements of the three-body states in $\Phi^J_{\gamma\lambda}$, we may rewrite Eq. (7) as

$$T^J_{nm} - K^J_{nm} = \frac{i}{2} \sum_{\gamma\lambda} \int T^J_{n\gamma} \Phi^J_{\gamma\lambda} K^J_{\lambda m} ds_\gamma ds_\lambda \; ; \tag{8}$$

here the stable two-body $\Phi^J_{\gamma\lambda}$ are

$$\Phi^J_{\gamma\lambda} = \frac{Q_\lambda}{4\sqrt{s}} \delta_{\gamma\lambda} \delta(s_\gamma - s) \, \delta(s_\lambda - s) \; . \tag{9}$$

For the diagonal three-body states we will still use the subscript γ, and they become

$$\Phi^J_{\gamma\lambda} = \frac{Q_\lambda q_\lambda}{4\sqrt{s}} \frac{\delta_{\gamma\lambda} \delta(s_\gamma - s_\lambda)}{4\sqrt{s_\gamma}} \; . \tag{10}$$

Henceforth we shall discuss a single partial wave, so we will drop the superscript J.

As it stands, Eq. (8) is an integral equation. We shall now make certain factorization assumptions that will reduce Eq. (8) to a matrix equation. It is clear that a matrix equation will be easier for practical calculations (i.e., fitting the isobar amplitudes). Indeed the factorization assumptions we make are already inherent in the isobar model. As in the isobar model, we assume $T_{\alpha\beta}$ to factor,

$$T_{\alpha\beta} = \tau_{\alpha\beta} f^*_\alpha f_\beta \; , \tag{11}$$

where f_α depends on barrier factors and final state factors of the isobar decay and $\tau_{\alpha\beta}$ is only a function of s.

In addition we assume $K_{\alpha\beta}$ can be factored in the same way:

$$K_{\alpha\beta} = k_{\alpha\beta} f^*_\alpha f_\beta \; , \tag{12}$$

where $k_{\alpha\beta}$ depends only upon s and is free from all branch points. In the spirit that the isobar model is describing particle states, we shall take $k_{\alpha\beta}$ to be a real function of s (or $W = \sqrt{s}$). If the several final

state resonance bands did not overlap, then a real k-matrix implies a symmetric T-matrix.

We can reduce the integral Eq. (8) to a matrix equation by substitution of $K_{\alpha\beta}$ and $T_{\alpha\beta}$; we thus obtain

$$\tau_{\alpha\beta} - k_{\alpha\beta} = \frac{i}{2} \sum_{\gamma\lambda} \tau_{\alpha\gamma} \Delta_{\gamma\lambda} k_{\lambda\beta} , \tag{13}$$

where for stable two-body states

$$\Delta\gamma_{\lambda} = \frac{Q_{\lambda} \delta_{\gamma\lambda} |f_{\lambda}|^2}{4\sqrt{s}} , \tag{14}$$

i.e., diagonal with value proportional to Q times barrier, and for three-body states

$$\Delta_{\gamma\lambda} = \int \Phi_{\gamma\lambda} f_{\gamma}^{*} f_{\lambda} \, ds_{\gamma} \, ds_{\lambda} . \tag{15}$$

one easily shows that Eq. (13) implies the usual unitarity relation $\tau - \tau^{+} = i\tau^{+}\Delta\tau$; see Appendix I.

We now discuss the barrier factor f_{λ}. For the terms which only involve stable particles, we assume that $|f_{\lambda}|^2$ is the Blatt-Weisskopf[8] barrier factor. Our confidence in these factors has recently been increased by Von Hippel and Quigg,[8] who showed that they can be derived from general properties of spherical harmonics and are not limited to square wells. But since our isobar does not have a fixed mass, we have to take its production barrier B_{α} (Q_{α}, L_{α}) weighted over the Dalitz plot. To be consistent with the isobar model used to obtain the amplitudes, we describe the final state interaction by the Watson final state interaction $(e^{i\delta_{\alpha}} \sin \delta_{\alpha} / q_{\alpha}^{\ell+1/2}) W_{\alpha}$. The δ_{α} is the phase shift for the elastic scattering amplitude A_{α}, representing the α isobar ($\pi N \to \pi N$ or $\pi\pi \to \pi\pi$), where $q_{\alpha}^{\ell+1/2}$ is approximately the square root of: q_{α} times the barrier for the elastic scattering. For a complete s-channel diagram showing all important factors see Fig. 1. Therefore, the form of f_{α} becomes

$$f_\alpha = W_\alpha B_\alpha (Q_\alpha, L_\alpha), \tag{16}$$

where B_α is the square root of the Blatt-Weisskopf barrier, L_α the production angular momentum of the isobar, and Q_α the c. m. production momentum of the isobar.

For the stable two body, f_α is equal to B_α and W_α is equal to one. In the case of the isobar, W_α becomes

$$W_\alpha = \frac{\dfrac{A_\alpha(s_\alpha)}{q_\alpha^{1/2} B_\alpha(q_\alpha, \ell_\alpha)}}{\left(\displaystyle\int_{(m_1+m_2)^2}^{(\sqrt{s}-m_3)^2} \frac{|A_\alpha|^2}{B_\alpha^2(q_\alpha, \ell_\alpha)} \frac{ds_\alpha}{4\sqrt{s_\alpha}} \right)^{1/2}}, \tag{17}$$

where A_α is the elastic scattering Argand amplitude $[0 < |A_\alpha| < 1]$, $B_\alpha(q_\alpha, \ell_\alpha)$ is the square root of the Blatt-Weisskopf barrier for formation, q_α is the c. m. momentum of particles that make up the isobar, and ℓ_α is the angular momentum of the particles that make up the isobar. The normalization is done because we treat W_α as a weighting function. For the A_α we take a Breit-Wigner form,

$$A_\alpha(s_\alpha) = \frac{q_\alpha \gamma_\alpha B_\alpha^2(q_\alpha, \ell_\alpha)}{E r_\alpha - \sqrt{s_\alpha} - i\gamma_\alpha q_\alpha B_\alpha^2(q_\alpha, \ell_\alpha)}. \tag{18}$$

If we define

$$T_\alpha(E_\alpha) = \frac{A_\alpha(E_\alpha)}{q^{1/2} B_\alpha(q_\alpha, \ell_\alpha)}, \tag{19}$$

where $E_\alpha = \sqrt{s_\alpha}$ then f_α becomes

$$f_\alpha = \frac{T_\alpha(E_\alpha)\, B_\alpha(Q_\alpha, L_\alpha)}{\left(\int_{m_1+m_2}^{E-m_3} |T_\alpha(E_\alpha)|^2 \, \frac{q_\alpha}{2} \, dE_\alpha \right)^{1/2}} . \tag{20}$$

In our Breit-Wigner form [Eq. (18)] Er_α and γ_α are constants given in units of pion masses. See Table I for a list of values used.

The diagonal terms of the Δ matrix become for isobar α,

$$\Delta_{\alpha\alpha} = \frac{1}{4\sqrt{s}} \frac{\int_{m_1+m_2}^{\sqrt{s}-m_3} |T_\alpha(E_\alpha)|^2 \, \frac{Q_\alpha q_\alpha}{2} \, B_\alpha^2 \, dE_\alpha}{\int_{m_1+m_2}^{\sqrt{s}-m_3} |T_\alpha(E_\alpha)|^2 \, \frac{q_\alpha}{2} \, dE_\alpha} . \tag{21}$$

We see that the normalization was chosen so that $\Delta_{\alpha\alpha}$ is essentially an average of $Q_\alpha B_\alpha^2/(4\sqrt{s})$, which is a dimensionless quantity. Therefore $K_{\alpha\beta}$ in Eq. (13) is a dimensionless number, and in fact the whole Eq. (13) is dimensionless.

In this paragraph we give an alternative prescription for $\Delta_{\alpha\alpha}$ which we did not use. This prescription will only change the K-matrix parameters and not the T-matrix which we fit to. One can think of the isobar being described by a relativistic Breit-Wigner resonance where the "typical" momentum of the isobar is given by

$$\overline{Q_\alpha} = \int_{m_1+m_2}^{\sqrt{s}-m_3} \frac{1}{N} \frac{\Gamma_{el}}{(s_R - E_\alpha^2)^2 + \Gamma_{total}^2} \frac{Q_\alpha q_\alpha}{2} \, dE_\alpha . \tag{22}$$

The Breit-Wigner is normalized all the way out to $\sqrt{s} = \infty$ such that

$$\int_{m_1+m_2}^{\infty} \frac{\Gamma_{el}}{(s_R - E_\alpha^2)^2 + \Gamma_{total}^2} \frac{q_\alpha}{2} dE_\alpha = N. \tag{23}$$

In this case, $\Delta_{\alpha\alpha}$ would become

$$\Delta_{\alpha\alpha} = \frac{1}{4\sqrt{s}} \int_{m_1+m_2}^{\sqrt{s}-m_3} \frac{1}{N} \frac{\Gamma_{el}}{(s_R - E_\alpha^2)^2 + \Gamma_{total}^2} \frac{Q_\alpha q_\alpha}{2} B_\alpha^2 dE_\alpha. \tag{24}$$

In making this assumption one is relying on the fact that as the width of the Breit-Wigner goes to zero it becomes a delta function. We have chosen our particular definition of $\Delta_{\alpha\alpha}$, Eq. (21), because it depends on the measured Argand amplitudes and is independent of model assumptions, unlike Eq. (24).

We assume that $k_{\alpha\beta}$ is real with no branch points and can be described by simple factorizable poles (which represent the formation of N^* resonance) plus nonfactorizable background terms which are polynomials in $\sqrt{s}$. The K-matrix program Kanal which was written to do the fits had the possibility for three regular poles and a background linear in $\sqrt{s}$ (which from now on we will call W). That is,

$$k_{\alpha\beta} = \sum_{r=1}^{3} \frac{\gamma_\alpha^r \gamma_\beta^r}{E_r - W} + C_{\alpha\beta} + W B_{\alpha\beta}. \tag{25}$$

We may express the cross section in terms of the reduced amplitudes τ_{1n}. Starting with Eq. (5) and taking only one partial wave and isobar, we obtain

$$\sigma_{1n}(W) = \frac{\pi}{4Q_1 W}\,(J+\tfrac{1}{2}) \int |T_{1n}(W,E_n)|^2 \;\frac{Q_n q_n\, dE_n}{8W} \tag{26}$$

By substitution of Eq. (11) and (20) into Eq. (26), we get

$$\sigma_{1n}(W) = \frac{\pi}{16Q_1 W^2}\,(J+\tfrac{1}{2}) \;\frac{\int |\tau_{1n}(W)|^2 \;\frac{Q_n q_n}{2} B_1^2 B_n^2 \,|T_n(E_n)|^2 dE_n}{\int |T_n(E_n)|^2 \;\frac{q_n}{2}\, dE_n}$$

Noting that $\tau_{1n}(W)$ and B_1^2 are independent of E_n, this becomes

$$\sigma_{1n} = \frac{\pi}{4Q_1^2}\,(J+\tfrac{1}{2})\,|\tau_{1n}(W)|^2\,\Delta_{11}\,\Delta_{nn}\,. \tag{28}$$

If the partial-wave S-matrix is defined by

$$S_{\alpha\beta} = \delta_{\alpha\beta} + 2i\,A_{\alpha\beta}, \tag{29}$$

the cross section is given by

$$\sigma_{1n} = \frac{4\pi(J+\tfrac{1}{2})\,|A_{1n}|^2}{Q_1^2}\,. \tag{30}$$

Therefore,

$$A_{1n} = \frac{\sqrt{\Delta_{11}}\,\sqrt{\Delta_{nn}}\,\tau_{1n}}{2}\,. \tag{31}$$

The A_{1n} amplitudes are the results of the isobar-model fit to $N\pi\pi$,[1] and the A_{11} amplitudes come from "EPSA" (elastic phases shift analysis).[2,3] The program Kanal was written to fit the A's by a χ^2

method, using the K-matrix parametrization of Eq. (25).

Before leaving the K-matrix formalism we indicate how we dealt with the fact that there are two delta isobars in the $N\pi\pi$ final state ($N\pi_1\pi_2 = \Delta_1\pi_2 + \Delta_2\pi_1$). We treated them as separate channels with the same coupling. This coupling was $\gamma_\Delta/\sqrt{2}$ where γ_Δ is the total delta coupling. Once we calculated the T's for the individual delta's, we added the amplitudes together as

$$T_\Delta = \frac{T_{\Delta_1}}{\sqrt{2}} + \frac{T_{\Delta_2}}{\sqrt{2}} \ . \tag{32}$$

3. DETERMINATION OF THE OVERALL PHASE AND SCALING OF ERRORS

In this section we discuss how we use the K-matrix to scale our statistical errors to more reasonable values. We also show how the intrinsic overall arbitrary phase of our isobar model amplitudes at a given energy can be removed by the K-matrix.

3.1 Scaling of Errors

In order to use the K-matrix, we needed to supplement our $N\pi\pi$ amplitudes A_{1n} with elastic amplitudes A_{11}. Two sets were available, those of CERN[2] and those of Saclay.[3] We made two separate fits, one using A_{11} (CERN) and one using A_{11} (Saclay). However, it is well known that the deviation between the two solutions are greater than the statistical errors; so we used larger errors in these fits. The errors, $\delta(A_{11})$, were calculated by taking the rms (root mean square) deviation between the two A_{11} solutions. For a few waves at some energies this external error was too small, so the statistical error claimed by Saclay analysis was used [no statistical error is quoted by CERN[2]]. For the inelastic errors it would be nice to again use external errors. However, our analysis is the only existing inelastic analysis available. Instead of

using our statistical errors which we felt were too small, we decided to scale our errors so that the inelastic and elastic data would contribute equally to the overall multichannel χ^2. For the purpose of scaling, errors we wanted to select a wave (or waves) that has one clear resonance in the elastic phase shift and where our inelastic fit is in good agreement with the elastic phase shift prediction. Resonances in the 1500-MeV region are not good candidates, because we are missing inelastic data from 1540 - 1650 MeV.* Resonances in the 1900 MeV are also poor candidates, since we have limited ourself to F waves in our model. This means we were unable to satisfactorily describe the peripheral production of pions that become important in this energy region.[1] The 1700-MeV resonance region seems ideal. In this region there are four resonances that are clearly seen in the EPSA: the S31, D33, D15, and F15. Since S31 and D33 resonate near 1650, they cannot be used because of the energy gap (see footnote). The D15 is not in as good agreement with EPSA as the F15. For this reason we only took the F15 wave to scale x^2-elastic with x^2-inelastic in our K-matrix fits.

The procedure was to adjust the errors on the inelastic amplitudes for the F15 until the χ^2 per energy bin was equal for the elastic and the inelastic contributions. We used only one pole and a constant background as parameters in the K-matrix and fit in the F15 partial wave energy region from 1585 to 1810 MeV with the inelastic amplitudes have one free phase at each energy. Notice that at this point we are only using the K-matrix to describe the moduli of the inelastic amplitudes.

---

*In our isobar model fits, we had a complete set of $N\pi\pi$ data from 1310 - 1970 MeV except for a gap of data from 1540 - 1650 MeV.

When we first fit with external errors on the elastic and raw statistical error on the inelastic, by far the greatest contribution to χ^2 the inelastic channels. As we scaled up the statistical errors on the inelastic amplitudes, the χ^2 began to shift to the elastic channel. At a scaling of three on the inelastic errors the χ^2 per bin of energy became equal for the elastic and inelastic contributions. Three seems like a large factor. However, if one looks at the statistical errors quoted by Bareyre at Batavia[3] and compares them with the external errors, one also finds a factor of from 2 to 4. So for the rest of the partial wave fits, we used three times the statistical errors for the inelastic amplitude and the external errors for the elastic.

3.2 Overall Phase

At each energy all the inelastic amplitudes are well determined with respect to each other but have an overall arbitrary phase. With the unitary constraint relating the elastic amplitudes to the inelastic amplitudes, we are now in a position to determine this phase at each energy. For this purpose we only consider dominant partial waves. See Fig. 2, which shows $(1-\eta^2)$ for the dominant waves. The D15 and the F15 which are two such, dominate partial waves in the energy region from 1585 - 1810 MeV; they show good resonant motion in the elastic channel, so we expect to see motion in the inelastic channel. This was our starting point for determination of the overall arbitrary phases in this energy region.

Our fitting program (Kanal) had the ability to fit with an unknown overall phase ϕ_i at the ith energy bin for the inelastic data. First we obtained a solution for F15 and D15 from 1585 to 1810 MeV (8 elastic + 5 inelastic bins). Here we used a single pole and a constant background as parameters in the K-matrix, with a free phase at each energy.

This fit was performed separately for both CERN and Saclay EPSA solutions for the elastic channel. This gave us five phases for CERN D15 and five phases for Saclay D15; we also had the same number of phases for F15. At this point we have four sets of phases at each energy. We want to reduce these four sets to only one set of phases that will equally describe the data for the different inputs: D15 (Saclay), F15 (Saclay), D15 (CERN), F15 (CERN). We accomplished this goal through an iterative process.

First we minimized the total D15 CERN and D15 Saclay χ^2 by introducing a single parameter Y. It had the property that if Y = 0, the phases are equal to D15 CERN phases, and if Y = 1, the phases are equal to D15 Saclay phases. The specific parametrization of the ϕ_i in terms of Y was

$$\phi_i = \phi(\text{D15 CERN})_i + Y\ (\phi(\text{D15 Saclay})_i - \phi(\text{D15 CERN})_i). \quad (33)$$

We assumed that χ^2_{total} (sum of two χ^2) is a quadratic function of Y:

$$\chi^2_{total} = \chi^2(1)\ \ (2Y^2-Y) + 4\chi^2(1/2)\ \ (Y-Y^2) + \chi^2(0)\ \ (2Y^2-3Y+1), \quad (34)$$

where $\chi^2(1)$ is the true total χ^2 at Y = 1, $\chi^2(1/2)$ is the true total χ^2 at Y = 1/2 and $\chi^2(0)$ is the true total χ^2 at Y = 0. The solution to the quadratic equation (34) that minimizes total χ^2 is

$$Y = \frac{\chi^2(1) - 4\chi^2(1/2) + 3\chi^2(0)}{4\chi^2(1) - 8\chi^2(1/2) + 4\chi^2(0)}. \quad (35)$$

By going through this procedure we arrived at one set of phases that minimized χ^2 for D15 CERN and D15 Saclay. The same procedure was repeated for the two sets of F15 phases (CERN and Saclay). We thus reduced the four sets of phases to only two. A final iteration using

Eqs. (33) and (35) yielded one set of phases. See Fig. 3, which gives a flow diagram of this iterative process.

Next we looked at the F35 and F37 waves which went from 1730 to 1970 in energy. In the overlap region (1730 - 1810) we minimized all four waves, each with two combinations, leaving the 1850 - 1970 phases free for the F35 and F37. However, this procedure did not change the overlap phases very much from the valves obtained by just considering D15 and F15.

After finally arriving at a set of phases from 1650 to 1810 we determined the phases from 1850 to 1970 just using F35 and F37, where one pole and constant background were again used in the K-matrix. Thus, we were able to arrive at nine phases for our nine upper energies.

We then turned to the lower energies from 1310 to 1540. In this region the D13 and P11 are dominant waves and are ideal for determining the phases. The problem here, however, was to find a solution that would continue across the energy gap. The D13 at 1540 is very inelastic, but by 1650 it is no longer very inelastic. On the other hand, the P11 stays very inelastic all the way through the energy region. For this reason the P11 was the only partial wave that could be used to make the connection across the gap. Once we continue across the gap we may use, as above, both D13 and P11 to determine phases below the gap.

With the upper energy phases fixed on the values determined above, we parametrized the K-matrix by two poles and a constant background. The pole positions in the K-matrix were initially set and held at 1490 and 1770 MeV (nominal positions of P11 resonances), and the lower phases where left free to vary. We fit over the entire energy range from 1370 to 2010 MeV in order to continue across the gap. This gave us a solution which was almost the same solution as the final one for the

P11 given in this paper. We later added a linear term to the background and let the pole positions in the K-matrix vary.

At the 1972 Batavia conference, Bareyre[3] announced that there may be two P11 resonances, one at 1390 and another at 1540. This possibility could spoil our ability to bridge the gap.

If we assumed another resonance at 1540; it might create an additional 180° rotation across the gap in our Argand diagram. To test this we added another pole and rotated the upper energies by 180°. The results of the fits are shown in Table II. We see that χ^2 per degree of freedom is worse with the extra pole. Also the χ^2 of the elastic channel alone is worse. In fact the increase in χ^2 for the elastic channel comes from the energy region, where we are missing inelastic data. For these reasons we have rejected the 1540 resonance of the P11 if we consider it would cause a 180° flip of our upper energy solution with respect to our lower energy solution. When more inelastic data become available, a more precise statement can be made about the second P11 resonance.

Having provided a continuation across the gap, we turn to the D13 solution which was also fitted in the same range (1310 to 2010) as the P11. For the D13 we used three poles and a constant and linear background. At this point the lower phases were determined with essentially the same procedure as was used in the upper energies [Eqs. (33) and (35)]. However, we broke the lower region up into two regions to give more flexibility to our simple model of minimizing total χ^2. (Notice that there are nine energies below the gap and nine above.)

4. K-MATRIX FITS

In this section we give the results of the K-matrix fits.

In order to fit the K-matrix to the elastic and inelastic amplitudes,

we used two different minimizing methods, one due to Rosenbrock[9] and the other to Davidon.[10] When the fit was far away from solution we used the Rosenbrock method, which was more economical. As the χ^2 came close to a minimum the Davidon method was used. This method converges simultaneously toward the minimum and toward the true variance matrix (error matrix).

For a summary of the results of the K-matrix fitting, see Table III, where the χ^2, energy range, K-matrix parameters, pole position, and partial widths are listed for each wave fitted by the K-matrix. In Fig. 4 we display Argand diagrams and partial wave cross sections for the elastic and inelastic channels. The smooth curve on the Argand diagrams is the amplitude obtained from the K-matrix when the description was possible. For the P31 and the P33, we did not try to make a K-matrix fit, because there was no evidence for resonances and we did not see all the inelasticity $N\pi\pi$ channel. Cross-hatched marks on the curve correspond to energies D, E, and F, etc. The arrows indicate the known resonances from EPSA.[2,3] To the right inelastic Argand diagram, we give the variation with energy of the square modulus of the wave. The total inelastic contribution in each elastic wave is compared with the sum of the inelastic contributions (ϕ) we observe ($\ast$), where the elastic amplitudes are those of CERN.[2] All Argand diagrams are now determined to within one overall sign. We have chosen the ΔPP11 to be up.

5. POLES IN THE T-MATRIX

In this section we discuss how Eqs. (13) and (11) are analytically continued into the complex energy plane. This continuation naturally leads to an analytic T-matrix except for complex branch points associated with the isobars and poles due to S-channel resonances.

5.1 Kinematics

Once the K-matrix fits were completed, we searched in the complex energy plane for poles which are identified with the different resonance states. Because the K-matrix generates simple poles in the T-matrix, the residue of the pole is factorizable. A simple proof of this is given in Appendix II. The residue matrix of the T-matrix pole is identified with the coupling of the resonant state to the different channels. One would like to relate this coupling matrix with the usual partial widths Γ of the resonance. The partial width is equal to the coupling times a kinematic factor. The question is, should this kinematic factor be evaluated at the pole or on the real axis? We decided to take the kinematics calculated on the real axis, because for a simple Breit-Wigner with narrow width, the partial width will be more real and the sum of the partial widths will be closer to the total width. See Appendix III.

5.2 Analytic Continuation

In order to search the complex energy plane for poles, we had to continue analytically the Δ_{mn} matrix into the complex plane. The off-diagonal terms of Δ_{mn} matrix turn out to be from 5% to 20% of the diagonal elements. Also they do not seem to add any additional analytic sheet structure, and it is very time-consuming to evaluate them many times. When we did the pole search, therefore, we set the off-diagonal terms of the Δ_{mn} matrix to zero.

In order to continue the Δ_{mn} matrix to complex energy W, we have to do a contour integration in the complex diparticle mass E_α plane related to a given isobar. Equation (21)

$$\Delta_{\alpha\alpha} = \frac{1}{4W} \frac{\int_{m_1+m_2}^{W-m_3} |T_\alpha(E_\alpha)|^2 \frac{Q_\alpha q_\alpha}{2} B_\alpha^2 \, dE_\alpha}{\int_{m_1+m_2}^{W-m_3} |T_\alpha(E_\alpha)|^2 \frac{q_\alpha}{2} \, dE_\alpha} . \tag{36}$$

When we are on the real axis, all terms in the integral are real. Since we want all terms to be analytic in E_α, we must be able to expand them in a Taylor series with real coefficients as a function of E_α. Every term in the integral is obviously analytic except $|T_\alpha|^2$. However, we know that T_α is analytic. In fact, T_α can be related to a function m_α, which is free from cuts, by

$$T_\alpha = \frac{1}{m_\alpha - iq_\alpha} . \tag{37}$$

Recall that T_α is essentially the $2 \to 2$ scattering amplitude, so that m_α is an inverse K-matrix. Therefore, $|T_\alpha|^2$ can be written as

$$|T_\alpha|^2 = \frac{1}{m_\alpha^2 + q_\alpha^2}, \tag{38}$$

which is obviously analytic.

5.2.1 The Pole in $|T_\alpha|^2$

Next we derive Eq. (41) to show that $|T_\alpha|^2$ has a pole, and that it occurs exactly where the sheet II pole occurs for the amplitude T_α of Eq. (37). We use the standard definition of sheets; the imaginary part of $q_\alpha > 0$ [< 0] corresponds to sheet I [II]. Therefore, dropping the α index, we have the usual relationships:

$$T_I(E) = \frac{1}{m(E) - iq_I(E)}, \quad T_{II}(E) = \frac{1}{m(E) - iq_{II}(E)},$$

$$m^*(E^*) = m(E), \quad q_I(E) = -q_I^*(E^*), \quad q_I(E) = -q_{II}(E), \quad q_{II}(E) = -q_{II}^*(E^*). \quad (39)$$

From Eqs. (38) and (39), we have

$$|T|^2 = \frac{1}{m^2(E) + q_I^2(E)} = \frac{1}{m^2(E) + q_{II}^2(E)} . \quad (40)$$

This can be written in a symmetric form using both sheets:

$$|T|^2 = \frac{1}{m(E) - iq_I(E)} \; \frac{1}{m^*(E^*) + iq_{II}^*(E^*)} = T_I(E)\, T_{II}^*(E^*)$$

$$= \frac{1}{m(E) - iq_{II}(E)} \; \frac{1}{m^*(E^*) + iq_{II}^*(E^*)} = T_{II}(E)\, T_I^*(E^*) . \quad (41)$$

Since $T(E)$ is the two-body elastic scattering amplitude of the particles that make up the isobar, it will have a pole on sheet II that is properly identified with the isobar, as we set out to show.

5.2.2 Contours of Integration

Notice that both integrals in Eq. (36) are path dependent because of the pole in $|T_\alpha|^2$. We can take many paths of integration. We are, however, only interested in the paths that go most directly to the end point of integration, because they lie near the physical region, which is just the real axis.

In Fig. 5 we have drawn three different paths of integration and labelled them with the symbols $\Delta, \Delta', \Delta''$ as used for the integrals themselves, and in Fig. 6 we have deformed the three contours to show that they differ only by circles around the pole. Also in Fig. 6 we show a branch cut coming to the end-point of integration which is due

to the factor Q in the integral in the numerator of Eq. (36). Along Δ' we want Q to be continuous; but this means that Q is on a different sheet when the integration passes near the pole. So in order to define on what sheet, $\Delta_{\alpha\alpha}$ is evaluated, we must specify both the sign of the imaginary part of Q at the lower limit of integration and also the path (Δ, Δ', or Δ'') of the integration. In summary of Figs. 5 and 6, we find six sheets generated by three contours (Δ, Δ', Δ'') and two possible signs for ImQ. However, we only expect to find poles on the sheets with ImQ < 0 for reasons of causality.

5.2.3 Sheets in W Plane

Next we point out that all values of Δ, Δ', and Δ'' approach zero if the end-point of integration ($W-m_3$) approaches E_{pole}. To see this, consider Eq. (36), which we write as $\Delta \equiv I/D$, Eq. (43). Then D diverges as the end-point approaches the pole (in $|T_\alpha|^2$). But the integrand of I contains a factor Q which always goes to zero at the end-point and cancels the divergence of $|T_\alpha|^2$. So at the end-point Δ equals a finite number divided by infinity, which is equal to zero. So as a function of W we have shown that the values of Δ (Δ, Δ', Δ'') all become equal at $W = E_{pole} + m_3$ so that $E_{pole} + m_3$ is the beginning of a branch cut (see Fig. 7). There is, of course, also a conjugate branch cut at $E = E^*_{pole} + m_3$, also drawn on Fig. 7.

Soon we shall discuss hunting in W, looking for a pole in T. Suppose we find a pole at W on the Δ sheet; there will in general be "shadow poles" at W' on the Δ' sheet and at W'' on Δ'', where W, W', W'' may be close. Hence we must understand the W sheet structure of Fig. 7 to decide which of the poles is most influential at real axis.

To understand Fig. 9, it is helpful to consider Fig. 8, a sketch of contours in the E plane. In Fig. 8, a dashed line starting at E_{pole} corresponds to the branch cut starting at $E_{pole} + m_3$ in Figs. 7 and 9. This line is no barrier to the contours Δ, Δ', Δ'', but we cannot move the end-point $W-m_3$ across this line without changing the names of the contour (changing sheets in the W plane).

Note that if $W-m_3$ is near the real axis the only short contour is Δ. Consequently the W sheet connecting to the physical region in Fig. 9 is labelled Δ.

To go further we need Fig. 8a through 8d. In Fig. 8a, the end point of the integral is below the dashed line. As we deform the contour from Fig. 8a to Fig. 8d, the end-point of the integral moves around the pole in the E plane. In Fig. 8d we are above the dashed line. If we consider point 3 in Fig. 9a and move it continuously up through the branch cut, we will change sheets. We see that the Δ contour in Fig. 8a deforms continuously into Δ' contour in Fig. 8d. Thus point 3 of Fig. 9a would move from the Δ sheet to the Δ' sheet, e.g., point 2 of Fig. 9b.

In Fig. 9a through 9c we show three points on each of the Δ, Δ', and Δ'' sheets. For each point we have drawn continuous paths leading to the physical region. In Fig. 9b and 9c, when we pass onto the Δ sheet (the only sheet connected to the physical region) the lines are dashed. The length of the lines in Fig. 9a through 9c are a measure of how close a point is to the physical region. Therefore if we find a pole on Δ, Δ', or Δ'', we can use Fig. 9 to tell us how close it is to the physical region.

In practice it is necessary to calculate only one contour integral. We now show how this is done. From Eq. (21), making energy

dependence explicit, we have

$$\Delta = \frac{\frac{1}{4W}\int_{m_1+m_2}^{W-m_3} |T(E)|^2 Q(W,E)\,\frac{q(E)}{2}\,B^2(W,E)\,dE}{\int_{m_1+m_2}^{W-m_3} |T(E)|^2\,\frac{q(E)}{2}\,dE}\,, \tag{42}$$

where the path of integration is Δ (see Fig. 5). Let us define

$$\Delta \equiv \frac{I}{D}\,, \tag{43}$$

where I is the main integral and D is the denominator of Eq. (42), respectively. Call the denominator residue R_D; then, by using Cauchy's integral formula for contours Δ and Δ'', we obtain

$$\begin{aligned} D - D' &= 2\pi i R_D = 2\pi i \lim_{E \to E_{pole}} (E_{pole} - E)\,|T_{(E)}|^2\,\frac{q(E)}{2} \\ I - I'' &= 2\pi i Q(W, E_{pole})\,B^2(W, E_{pole})\,R_D\,. \end{aligned} \tag{44}$$

We must be sure that we evaluate $Q(W, E_{pole})$ on the correct sheet. It is clear, if we know Δ, R_D, and D, that we can evaluate Δ'' by

$$\Delta'' = \frac{I''}{D''} = \frac{I - 2\pi i\,Q(W, E_{pole})\,B^2(W, E_{pole})\,R_D}{D\left(1 - \frac{2\pi i R_D}{D}\right)} \tag{45}$$

Thus it is clear from Eq. (45) that

$$\Delta'' = \frac{\Delta - 2\pi i\,Q(W, E_{pole})\,B^2(W, E_{pole})\,R_D/D}{1 - 2\pi i R_D/D}\,.$$

In the case of Δ' the spiral around E_{pole} is counterclockwise (see Figs. 5 and 6), so $2\pi i \to -2\pi i$, and that is the only change in the denominator D.

In addition in the main integral I, Q changes sign because it is on the other sheet (see Fig. 6), so we obtain

$$\Delta' = \frac{\Delta - 2\pi i\, Q(W, E_{pole})\, B^2(W, E_{pole})\, R_D/D}{1 + 2\pi i\, R_D/D} \quad . \tag{47}$$

[In this aside we compare the sheet structure generated by $\Delta_{\alpha\alpha}$ of Eq. (24) (reliance on relativistic Breit-Wigner). It is clear that the sheet structure we have discussed so far generated by Eq. (21) is a spiral sheet structure. We see that since Eq. (24) does not have a denominator, Δ' would be equal to Δ''. Therefore this sheet structure would be square root in nature.]

Another property which may be demonstrated is that

$$\Delta(W) = -\Delta(W^*) \tag{48}$$

for all three contours Δ, Δ', Δ'' and both signs of Q. It is also clear that Q in the integral Δ has the property

$$Q(W, E) = -Q^*(W^*, E^*) \tag{49}$$

for a given imaginary part of Q. This follows from

$$Q^2(W, E) = Q^2(W^*, E^*). \tag{50}$$

All other terms that appear in the integral, Eq. (21), are Hermitian. Thus they are the complex conjugate of the value above the real axis when they are integrated below the real axis. So from Eq. (21), it is clear that

$$\frac{\frac{1}{4W}\int_{m_1+m_2}^{W-m_3} |T(E)|^2 Q(W,E)\frac{q(E)}{2} B^2(W,E)dE}{\int_{m_1 m_2}^{W-m_3} |T(E)|^2 \frac{q(E)}{2} dE} =$$

$$-\left(\frac{\frac{-1}{4W^*}\int_{m_1+m_2}^{W^*-m_2} |T(E)|^2 Q(W^*,E)\frac{q(E)}{2} B^2(W^*,E)dE}{\int_{m_1+m_2}^{W^*-m_3} |T(E)|^2 \frac{q(E)}{2} dE}\right)^* . \quad (51)$$

Therefore Eq. (49) is true by the way we constructed our integrals.

5.3 Poles

To demonstrate sheets and poles in our model, we will take the F15 amplitude as an example. The F15 resonance lies near the ρN threshold which is $\sqrt{s}$ = (1700 - i54) MeV as shown in Fig. 10. When we did the T pole search we found F15 poles on each (Δ,Δ',Δ'', for ImQ < 0) sheet. The pole on the sheet generated by the Δ contour is closest to the physical region. Figure 10 shows the sheet structure and continuous paths going to the different poles on the different sheets. The poles and corresponding sheets are (1672-i77)Δ, (1682-i54)Δ', and (1682-i84)Δ''. The path from the physical region to the pole on the Δ'' sheet is drawn in such a way as to reveal the path moving from the Δ sheet to the Δ'' sheet as it crosses the branch cut. All poles that we report in this paper are the closest poles to the physical region.

Once the pole position was found, we propagated the error matrix from the K-matrix fit to an error matrix for the pole position by dotting the Jacobian matrix and its transpose into the K-matrix fit error matrix.

$$\sigma^2_{Pij} = \left(\frac{\partial X_{Pi}}{\partial X_{K\ell}}\right)^T \sigma^2_{K\ell m} \left(\frac{\partial X_{Pj}}{\partial X_{Km}}\right), \tag{52}$$

where $\sigma^2_{K\ell m}$ is the K-matrix fit error matrix, and σ^2_{Pij} is the pole position 2X2 error matrix (real and imaginary). X_{Pi} is the pole position vector (only two components), $X_{K\ell}$ is the K-matrix variable, and $\partial X_{Pi}/\partial X_{K\ell}$ is the Jacobian matrix which was evaluated numerically. This procedure gave errors that were much too small when compared with the difference in pole position obtain from CERN and Saclay elastic inputs. The reason for this may be that the Davidon error matrix may not describe the true errors of our complicated space.

Table IV gives a summary of the T-matrix poles and the partial width calculated from coupling residue matrix times the kinematics on the real axis. The sign in the upper right corner of the box where the partial width is shown comes from the off-diagonal terms of the residue matrix and is related to the sign of the coupling. Since the Argand diagrams are determined to within one overall sign, the same is true for off-diagonal residue terms. We defer further discussion of these parameters until Sec. 6.

6. BREIT-WIGNER REFIT

In this section we discuss how we refit the smooth T-matrix obtained form the K-matrix fit with an amplitude which is a sum of a unitary background and a Breit-Wigner, rotated in such a way as to insure unitarity for the total amplitude. Once we have done the refits, we compare resonance parameters obtained from the K-matrix, the

T-matrix poles, and the Breit-Wigner refit. The motivation for these comparisons was to find out how sensitive resonance parameters are to the prescription from which they are obtained.

6.1 U(UB + BW) Amplitude

In the past, resonances were parametrized by the Breit-Wigner form. The Breit-Wigner by itself is unitary. Since there is always a background present due to other singularities, the T-matrix is in general a sum of Breit-Wigner plus background. Because this is not a manifestly unitary prescription, we have turned to the K-matrix. Now that we have made K-matrix fits and obtained smooth description of the data, we would like to know what the Breit-Wigner parameters are for comparison with theoretical predictions. For this purpose we used a unitary amplitude which was a Breit-Wigner plus a unitary background with no local poles. For convenience we denote this amplitude by U(UB + BW). We believe that the background should not be affected locally by the presence of the resonance. Therefore, the assumption that it is unitary with no local poles seems reasonable. In order to construct U(UB + BW), we let the Breit-Wigner be rotated by energy dependent phases (we believe that the Breit-Wigner not the background must accommodate itself to unitarity). These phases are calculated by the Davies-Baranger[11] constraint equation; also, see Goebel and McVoy.[11] Once we have made a K-matrix fit, we then refit using U(UB + BW) to the smooth T-matrix in the region of the pole, in order to extract the Breit-Wigner parameters.

Let us assume we have a unitary background S matrix B_{ij}, and a Breit-Wigner given by

$$R_{ij} = \frac{\frac{1}{2}\Gamma_i\Gamma_j}{(ER-E) - \frac{i}{2}\sum_k \gamma_k^2 Q_k}, \quad \text{where} \quad \Gamma_j = Q_j^{\frac{1}{2}}\gamma_j e^{i\theta_j}, \tag{53}$$

where all terms are real except Γ_j, and Q_j is the same as the diagonal terms of the Δ_{ij} matrix used in the K-matrix (see Eq. 21).

The Davies-Baranger constraint equation is

$$B_{ij}\Gamma_j^* = \Gamma_i. \tag{54}$$

Let us recall B_{ij} in term of the background T-matrix T:

$$B_{ij} = \delta_{ij} + 2iQ_i^{1/2}Q_j^{1/2}T_{ij}. \tag{55}$$

Now if we substitute Eqs. (53) and (55) into Eq. (54), we obtain

$$\sum_j (\delta_{ij} + 2iQ_i^{1/2}Q_j^{1/2}T_{ij})\gamma_j Q_j^{1/2} e^{-i\theta_j} = \gamma_i Q_i^{1/2} e^{i\theta_i}, \tag{56}$$

which can be shown to equal to

$$\gamma_i \sin\theta_i = \sum_j Q_j\gamma_j T_{ij} e^{-i\theta_j}. \tag{57}$$

The right-hand side of the Eq. (57) seems at first to be a complex number, but the left-hand side is real. So we can set the imaginary part of the right-hand side equal to zero; i.e.,

$$\sum_j Q_j\gamma_j \,\mathrm{Imag}(T_{ij})\cos\theta_j - \sum_j Q_j\gamma_j \,\mathrm{Real}(T_{ij})\sin\theta_j = 0. \tag{58}$$

At this point we assume that Q_i is real. This means we must restrict ourselves to energies such that the jth channel is open ($Q_j^2 > 0$). We now define the vectors

$$(\mathrm{Sin}) = \begin{pmatrix} \sin\theta_1 \\ \sin\theta_2 \\ \cdot \\ \cdot \\ \cdot \end{pmatrix} \quad \text{and} \quad (\mathrm{Cos}) = \begin{pmatrix} \cos\theta_1 \\ \cos\theta_2 \\ \cdot \\ \cdot \\ \cdot \end{pmatrix} \tag{59}$$

and the matrices

$$(\text{Real}) = \begin{pmatrix} Q_1\gamma_1\text{Real}(T_{11}) & Q_2\gamma_2\text{Real}(T_{12}) \cdots \\ Q_1\gamma_1\text{Real}(T_{12}) & Q_2\gamma_2\text{Real}(T_{22} \cdots \\ \vdots & \vdots \\ \vdots & \vdots \end{pmatrix}$$

and

$$(\text{Imag}) = \begin{pmatrix} Q_1\gamma_1\text{Imag}(T_{11}) & Q_2\gamma_2\text{Imag}(T_{12}) \cdots \\ Q_1\gamma_1\text{Imag}(T_{12}) & Q_2\gamma_2\text{Imag}(T_{22}) \cdots \\ \vdots & \vdots \\ \vdots & \vdots \end{pmatrix}. \tag{60}$$

Equation (58) then becomes

$$(\text{Imag})\,(\text{Cos}) - (\text{Real})\,(\text{Sin}) = 0 \tag{61}$$

or

$$(\text{Cos}) = (\text{Imag})^{-1}(\text{Real})\,(\text{Sin})\,. \tag{62}$$

In addition we have the added constraints between the sine and the cosine.

$$\text{Cos}^2\theta_i + \text{Sin}^2\theta_i = 1\,. \tag{63}$$

Unfortunately we were unable to solve these transcendental equations in general. Therefore we imposed Eqs. (62) and (63) by a χ^2 constraint and parametrized θ_i as a polynomial in W.

We were also interested in looking for the pole in T = U(UB + BW), (which is just the pole in the Breit-Wigner term) in the complex W plane. Since the U(UB + BW) amplitude must be Hermitian, θ_i must have the same real axis cut structure as Q_i[or Δ_{ii}; see Eq. (48)]. Therefore a natural parametrization for θ_i would be

$$\theta_i(W) = Q_i(W) \sum_{n=0}^{m} a_n W^n. \tag{64}$$

6.2 D15, F35, and F15 Refit

Having established this machinery, we performed a series of K-matrix fits and Breit-Wigner refits on three well-established resonances which were coupled to two, three, or four channels. We used the D15, F35, and F15 resonances. The results of these fits and refits are given in Table V. In line one of Table V we have identified the pole term of the K-matrix with Breit-Wigner-like resonance parameters: the mass is the location of the pole, Er, the ith partial width is just (kinematics)$\times \gamma_i^2$, and the total width is the sum of the partial widths. From this K-matrix fit we looked at the T-matrix pole where the real part of the pole position is identified with a mass; twice the imaginary part is identified with the total width (pole position is recorded in the mass column of Table V). From the residue of the T-matrix pole we defined the partial width as discussed in first part of Sec. 5. We record the real part, the imaginary part, and the modulus of partial width in Table V. For the total width we record the sum of the real parts, the imaginary parts, and the moduli of each partial width. For this T-matrix we do a U(UB + BW) refit from one-half width before the pole (in the T-matrix) to one-half width after the pole. We then obtain Breit-Wigner parameters (mass, partial widths, total width) which we record in Table V. For the Breit-Wigner term of the refit, we look at the pole in the complex W plane thus recording the pole position and residue-related partial widths as we did for the T-matrix. Next we refit the T-matrix again, but this time relaxing the Davies-Baranger constraint, thus performing a UB + BW refit where the θ_i's

are now constant with energy. From this Breit-Wigner refit we record the fitted parameters and the pole parameters. Finally we went back to the K-matrix fit and took out all the inelastic amplitudes, thus performing a fit only to the elastic data.[2,3] In order to absorb the inelastic part we added an unconstrained $\Delta\pi$ channel. We then went through the same series of refits and pole searches except for leaving out the U(UB + BW), since we only wanted to fit the elastic channel.

Figure 11 shows the Argand diagrams obtained from the U(UB + BW) refit to the F35 wave. The solid line is the total amplitude from 1740 to 1900 MeV (one-half width below T-matrix pole to one-half width above). The dashed line is the background for the same energy range. Arrows show the direction of increasing energy. Let us define $\Delta\theta_i$ as the change of rotation angle θ_i of the Breit-Wigner over the range of refit. Then

$$\Delta\theta_i = \theta_i(W = |W_{pole}|) - \theta_i\,[W = |W_{pole}| - 2\mathrm{Im}(W_{pole})] \qquad (65)$$

where W_{pole} is the pole position in the T-matrix. $\Delta\theta_i$ is plotted next to the elastic Argand diagrams of Fig. 11.

The results for the three resonances for both CERN and Saclay EPSA input are listed in Table V. Note that the pole position and residues for the T-matrix from both the K-matrix and U(UB + BW) are very close to each other. This is similar to the observation of Ball and Shaw[12] for the P33 resonance of the Nπ system. Also, the K-matrix parameters for the F35 have very little to do with the actual resonance parameters. This is because the background term in the K-matrix is very large, and we have shown in Appendix V that the background term couples directly into the pole position of the T-matrix. The resonance parameters obtained from T-matrix poles and

U(UB + BW) refits are the best candidates for checking theoretical predictions. Since they disagree by factors of 2 with each other, we would not expect theory to do any better.

7. SIGN OF COUPLINGS

In this section we discuss one possible prescription for extracting the signs of the couplings to the different channels from the total T-matrix near the resonant energies. The determination of these is important for the purpose of comparison with theory.

In order to understand what the sign of the resonance couplings is, one must know the exact Clebsh-Gordon coefficients that go into the isobar model fitting program. For all sign conventions see Chasmore-Herndon-Söding.[13] Once these conventions are known it might be possible to read the signs off the Argand amplitudes shown in Fig. 4. However, one sees that the resonance is not necessarily pointing up or down. In these cases one could do a unitary Breit-Wigner refit to determine the sign of the resonance coupling. However, this is really not necessary, because if we can see the resonance shape we should be able to guess the angles θ_i that the resonance is rotated by. We see, from Eq. (54) that the angles should be measureable by comparing the elastic and the inelastic channels. In the elastic channel (A11) the resonance is rotated by $2\theta_1$, and in the inelastic channels (A1i) the resonance is rotated by $\theta_1+\theta_i$. It is clear that θ_i has a range from -90° to 90°. Thus by determining these angles we will determine the sign of the couplings. We have seen that once we have made the unitary Breit-Wigner refit, the total T-matrix produced by this method is very close to the T-matrix produced by the K-matrix.

Thus we shall employ the simple interpretation of U(UB + BW) but determine the coupling sign directly from the T-matrix elements

produced by the original K-matrix fits. In fact for all resonant waves which have been fitted, we have looked at the T-matrix for all the elastic (including, e.g., $\Delta\pi \rightarrow \Delta\pi$) and inelastic channels and determined by eye what the nominal values of the θ's are. Table VI gives a list of the signs of the couplings and the angles from this eyeball-fit. If the nominal value of θ is within $\pm 30°$, we think we are safe in determing the sign. But if the value of θ is greater than $\pm 60°$, the sign is questionable.

8. PREDICTED CHANNELS

In this section we discuss two K-matrix fits in which we introduced an extra channel in order to make up for the lack of cross section observed in the $N\pi\pi$ system. In the S11 wave we know[14] there must be a component of $N\eta$. In the F37 wave we assumed that the additional channel was $N\pi\pi\pi$.

The upper right-hand plot for each incoming partial wave in Fig.4.1 through 4.16 gives the unitary check, i.e., a comparison between $\pi\lambda^2(J+1/2)(1-\eta^2)$ from EPSA (CERN[2]) and $N\pi \rightarrow N\pi\pi$ cross section contributed by each of the channels plotted in the right-hand column. Of the 13 incoming partial waves plotted, unitarity is well satisfied in 10 cases. We now discuss the other three.

The P31 has no evidence for resonance structure and such a small section observed in the isobar amplitudes that we did not do a K-matrix fit.

Around 1520 MeV a sizeable amount of cross section goes into $N\eta$ (about 4 mb). In our K-matrix fit to S11 we included the $N\eta$ channel[14] as a predicted channel (i.e., no input amplitude to constrain the χ^2). Our results are consistent around 1520 with all the $N\eta$ cross section going into the S11 wave. Figure 9 shows the total $N\eta$ cross section

plotted along with the S11 cross section of the $N\eta$ channel from the K-matrix. The S11 amplitude for the $N\eta$ predicted from the K-matrix is seen in Fig. 4.2. We believe that the moments of the $N\eta$ can be explained by an introduction of a few percent in cross section of P, D, and F waves in the region 1520 to 1590 (see Appendix VI).

In the 1900 region we do not saturate the inelasticity of the F57 wave by 3 mb, so we introduced a predicted channel. In this energy region, 1900-2000 MeV, the $N\pi\pi\pi$ cross section grows from 4 to 6 mb,[15] so we made the predicted channel an F37 decaying by $\Delta\rho$ with angular momentum in a P wave. Thus our analysis forces a prediction of the amplitude for F37 decaying into the $N\pi\pi\pi$ via a $\Delta\rho$ decay in a P wave. The predicted Argand amplitude is shown in Fig. 1.16.

9. CONCLUSIONS

We were able to apply the constraints of unitarity (using the K-matrix) to isobar-model-generated amplitudes. We obtained a good representation of the Argand diagrams in almost all channels. These permitted us to remove the overall phase uncertainty of the inelastic amplitudes at each energy.

With a good representation of the T-matrix we then could extract the pole parameters associated with resonant behavior in the Argand diagrams. The uniqueness of the pole parameters was demonstrated by doing Breit-Wigner refits to the fitted T-matrix amplitudes. Thus we found the same pole parameters in this alternative prescription. However, these refits showed it was not possible in general to relate pole parameters unambiguously to the parameters of the Breit-Wigner. Furthermore, the success of the refits and the obvious interpretation of the amplitude U(UB + BW) (of Sec. 6) justified a simple determination of coupling signs from the fitted T-matrix (K-matrix-generated) amplitudes.

Since the isobar model amplitudes may not be the final set the world accepts, the numbers presented here are subject to some changes. The biggest change may come from $N\pi\pi$ data in the energy gap. In addition theoretical predictions are stimulating searches for new solutions, using additional partial waves that may have been removed by the techniques described in Ref. 1.

ACKNOWLEDGMENTS

I wish to thank my advisor, Art Rosenfeld, for his guidance and support. I also want to thank all the physicists with whom I worked: Roger Cashmore, Gerard Smadja, Thomas Lasinski, and David Leith. Special thanks to Gerard and Tom for spiritual guidance.

My thanks to my fellow graduate students on this experiment, Larry Miller and David Herdon.

Finally I want to thank the other members of my thesis committee, William Chinowsky and Lawrence Ruby.

FOOTNOTE AND REFERENCES

*Work done under the auspices of the U. S. Atomic Energy Commission.

1. D. Herndon et al., A Partial Wave Analysis of the Reaction $\pi N \to \pi\pi N$ in the c. m. Energy Range 1300-2000 MeV. XVIth International Conference on High Energy Physics, Chicago, Illinois, Sept. 1972.

2. S. Almahed and C. Lovelace, Nucl. Phys. B40, 157 (1972).

3. R. Ayed, P. Bareyre, and Y. Lemoigne, contributed paper to the XVIth International Conference on High Energy Physics, Chicago, Illinois, Sept. 1972.

4. L. R. Miller (Ph. D. thesis), Lawrence Berkeley Laboratory Report LBL-38 (1971).

5. D. J. Herndon (Ph. D. thesis), Lawrence Berkeley Laboratory Report LBL-544 (1972).

6. P. Chavanon, Paris (Ph. D. thesis), Study of $p\pi \to p\pi^+\pi^0$ from 1.6 to 2 GeV, (1971) p. 16, Equation II-8.

7. P. Graves Morris, Nuovo Cimento 54, 818 (1968).

8. J. M. Blatt and V. F. Weisskofp. Theoretical Nuclear Physics (Wiley, New York, 1956), p. 361. See also F. Von Hippel and C. Quigg, Phys. Rev. B 5, 624 (1972).

9. H. H. Rosenbrock, Comp. J. 3, 175 (1960).

10. W. C. Davidon, Comp. J. 10, 406 (1968).

11. K. T. R. Davis and M. Baranger, Ann. Physik 19, 383 (1962). See Also C. J. Goebel and K. W. McVoy, Phys. Rev. 164, 1932 (1967).

12. J. S. Ball et al., Residue of $\pi N3$-3 Resonance Pole. National Science Foundation, Technical Report No. 72-69 (1973).

13. Cashmore-Herndon-Söding, The Extended Isobar Model, Lawrence Berkeley Laboratory Report LBL-543 (1973).

14. Y. Lemoigne et al., $\pi^- p \rightarrow \eta n$ Up to $P_\eta^{\pm} = 400$ MeV/c, Purdue conference on Baryon Resonances, April 1973.

15. E. Flaminio et al., Compilation of Cross Sections IV $-\pi^+$ Induced Reactions, CERN/HERA 70-5, Sept. 1970.

16. R. Cool and R. Marshak, Advances in Particle Physics, Vol. 2. (Wiley, New York, 1968), Chap. 2, p. 226.

APPENDIX I

UNITARITY OF THE τ-MATRIX

In this appendix we show that the τ-matrix as defined in the text by Eq. (13) is unitary, since we relate τ to S by Eqs. (29) and (31):

$$S = 1 + i\sqrt{\Delta}\ \tau\ \sqrt{\Delta} \quad .$$

(with no factor 2 in second term), the unitary condition to be tested is

$$\tau - \tau^+ \stackrel{?}{=} i\,\tau^+\,\Delta\tau \ . \tag{I.1}$$

Equation (13) from Sec. 2 is

$$\tau - k = i/2\ \tau\Delta k, \tag{I.2}$$

By definition the k-matrix is real and the Δ-matrix is Hermitian. As seen from Eq. (15) of Sec. 2:

$$\Delta_{\gamma\lambda} = \int \Phi_{\gamma\lambda} f^*_\gamma f_\lambda dS_\gamma dS_\lambda \tag{I.3}$$

$\Phi_{\gamma\lambda}$, which is the recoupling coefficient has the property that $\Phi_{\gamma\lambda} = \Phi^*_{\lambda\gamma}$ (Ref. 6). If we solve Eq. (I.2) for the τ-matrix, we obtain

$$\tau = k\ (1 - i/2\ \Delta k)^{-1} \ . \tag{I.4}$$

Let us substitute Eq. (I.4) into the left-hand side of Eq. (I.1); we get

$$k(1 - \tfrac{i}{2}\,\Delta k)^{-1} - (1 + \tfrac{i}{2}\,k\Delta^+)^{-1}k \stackrel{?}{=} i\tau^+\Delta\tau \ . \tag{I.5}$$

The next step is to introduce the unit matrices within [ ], in the appropriate places in the left-hand side of Eq. (I.5):

$$\left[(1+\tfrac{i}{2}\,k\Delta^+)^{-1}(1+\tfrac{i}{2}\,k\Delta^+)\right] k(1-\tfrac{i}{2}\,\Delta k)^{-1} - (1+\tfrac{i}{2}\,k\Delta^+)^{-1}\,k\left[(1-\tfrac{i}{2}\,\Delta k)(1-\tfrac{i}{2}\,\Delta k)^{-1}\right]$$

$$\stackrel{?}{=} i\tau^+\Delta\tau \ . \tag{I.6}$$

We have $(1-\frac{i}{2}\,k\Delta^+)^{-1}$ at the left of both terms, and a similar common factor on the right; factoring these out, we have

$$(1+\tfrac{i}{2}\,k\Delta^+)^{-1}\left[(1+\tfrac{i}{2}\,k\Delta^+)k - k(1-\tfrac{i}{2}\,\Delta k)\right](1-\tfrac{i}{2}\,\Delta k)^{-1} \stackrel{?}{=} i\tau^+\Delta\tau. \tag{I.7}$$

Simplifying, we obtain

$$(1+\frac{i}{2}k\Delta^{+})^{-1}\quad\frac{ik\Delta^{+}k}{2}+\frac{ik\Delta k}{2}\cdot\ (1-\frac{i}{2}\Delta k)^{-1}\stackrel{?}{=} i\tau^{+}\Delta\tau \tag{I.8}$$

Since Δ is a Hermitian matrix, we have

$$i(1+\frac{i}{2}k\Delta^{+})^{-1}k\Delta k(1-\frac{i}{2}\Delta k)^{-1} = i\tau^{+}\Delta\tau\ . \tag{I.9}$$

Finally, from Eq. (I.4) we note that the matrices following Δ are just τ and the matrices preceding Δ are τ^{+}. Indeed Eq. (I.1) is satisfied.

APPENDIX II

FACTORIZABLE RESIDUES

In this appendix we show that simple poles in the T-matrix have factorizable residues.

The first step is to demonstrate that a factorizable matrix has only one non-zero eigenvalue. Consider a matrix B which has only one non-zero term B_{11}. Let U_{ij} be a unitary matrix. Consider the matrix B' such that

$$B' = U^{+}BU\ . \tag{II.1}$$

Using the condition that only the B_{11} term is non-zero, we obtain

$$B'_{ij} = U^{*}_{1i}B_{11}U_{1j} \tag{II.2}$$

or, rewritten another way,

$$B'_{ij} = (U^{*}_{1i}\sqrt{B_{11}})\,(\sqrt{B_{11}}\,U_{1j}) \tag{II.3}$$

It follows from Eq. (II.3) that

$$B'_{ii}\,B'_{jj} = (B'_{ij})^{2}\ . \tag{II.4}$$

We shall use this result shortly.

It is clear that when we have a pole in the T-matrix, the determinant of T^{-1} will be zero. We may diagonalize T^{-1} with a unitary matrix U.

$$T_D^{-1} = \begin{pmatrix} \lambda_1 & & & \\ & \lambda_2 & & \\ & & \lambda_3 & \\ & & & \ddots \end{pmatrix} . \tag{II.5}$$

The determinant $\mathrm{Det}(T_D^{-1})$ becomes

$$\mathrm{Det}(T^{-1}) = \lambda_1 \lambda_2 \lambda_3 \cdots . \tag{II.6}$$

If we have a simple zero at complex total-center-of-mass energy $E = E_0$, then only one eigenvalue is equal to zero. By contrast a dipole (higher order pole) would have two (many) zero eigenvalues. Therefore we may assume that one eigenvalue is given by

$$\lambda_1 = C(E - E_0) \tag{II.7}$$

and the others are non-zero.

Therefore the diagonal T^{-1}-matrix can be written

$$T^{-1} = \begin{pmatrix} C(E - E_0) & & & \\ & \lambda_2 & & \\ & & \lambda_3 & \\ & & & \ddots \end{pmatrix} \tag{II.8}$$

and the inverse is

$$T_D = \begin{pmatrix} \frac{1}{C(E - E_0)} & & & \\ & \frac{1}{\lambda_1} & & \\ & & \frac{1}{\lambda_2} & \\ & & & \ddots \end{pmatrix} \tag{II.9}$$

The diagonal residue matrix is defined as

$$R_D = \lim_{E \to E_0} (E - E_0)\, T_D . \tag{II.10}$$

From Eqs. (II.9) and (II.10), we get

$$R_D = \lim_{E \to E_0} \begin{pmatrix} \frac{1}{C} & & \\ & \frac{(E-E_0)}{\lambda_2} & \\ & & \frac{(E-E_0)}{\lambda_3} \end{pmatrix} = \begin{pmatrix} \frac{1}{C} & & \\ & 0 & \\ & & 0 \end{pmatrix} . \qquad \text{(II.11)}$$

Notice that the non-diagonal residue matrix is just

$$R = U^{+} R_D U . \qquad \text{(II.12)}$$

From Eq. (III.4) we know that it factorizes.

APPENDIX III

POLE AND RESIDUE FOR A SIMPLE BREIT-WIGNER

In this appendix we discuss the shift of the pole parameters from the mass and width parameters of the Breit-Wigner. Also we discuss possible definitions of the residue and how it is related to the width.

For simplicity we take a single-channel T-matrix which is generated by a K-matrix:

$$T = \frac{K}{1 - i\Delta K} , \qquad \text{(III.1)}$$

where Δ is the kinematic factor. If we want a simple S-wave Breit-Wigner, we need a simple pole in the K-matrix without any barrier factors. Therefore we have

$$K = \frac{\Gamma/2}{E_R - E} , \qquad \text{(III.2)}$$

where E is the total c.m. energy and E_R is the K-matrix pole position. For Δ let us take a form that has a square root behavior and is equal to one at $E = E_R$:

$$\Delta = \sqrt{\frac{E}{E_R}} . \qquad \text{(III.3)}$$

Substituting Eqs. (III.2) and (III.3) into (III.1), we obtain

$$T = \frac{1}{\frac{E_R - E}{\Gamma/2} - i\sqrt{\frac{E}{E_R}}} \tag{III.4}$$

We know that we will have a pole in T when we have a zero in D(E), the denominator of T. Let E_P be the value of E where D(E) is equal to zero:

$$D(E_P) = 0 . \tag{III.5}$$

Therefore

$$\frac{E_R - E_P}{\Gamma/2} = i\sqrt{\frac{E_P}{E_R}} . \tag{III.6}$$

Squaring both sides of Eq. (III.6), we obtain

$$E_P^2 - 2\left(E_R - \frac{\Gamma}{8E_R}\right)E_P + E_R^2 = 0 , \tag{III.7}$$

which can be solved by the binomial theorm

$$E_P = E_R\left(1 - \frac{\Gamma^2}{8E_R^2}\right) \pm \frac{i\Gamma}{2}\sqrt{1 - \frac{\Gamma^2}{16E_R^2}} . \tag{III.8}$$

If we make the narrow width approximation ($E_R >> \Gamma$), Eq. (III.8) becomes

$$E_P = E_R\left(1 - \frac{\Gamma^2}{8E_R^2}\right) \pm \frac{i\Gamma}{2}\left(1 - \frac{\Gamma^2}{32E_R^2}\right) . \tag{III.9}$$

Taking the root with the minus sign because we want the pole to be on the correct sheet, we see that E_P is given by

$$E_P = E_R\left(1 - \frac{\Gamma^2}{8E_R^2}\right) - \frac{i\Gamma}{2}\left(1 - \frac{\Gamma^2}{32E_R^2}\right) . \tag{III.10}$$

The real part of the pole position has been shifted by $-\Gamma^2/8E_R$ from the K-matrix pole position. Also the width as been reduced in size by $\Gamma^3/32E_R^2$.

Next we expand D(E) in a Taylor series about E_P,

$$D(E) = - \left.\frac{\partial D}{\partial E}\right|_{E_P} (E_P - E) + \cdots , \qquad \text{(III.11)}$$

recalling that $D(E_P) = 0$. Differentiation of D(E) and Eq. (IV.11) yields

$$D(E) \approx \left(\frac{2}{\Gamma} + \frac{i/2}{\sqrt{E_P E_R}} \right) (E_P - E) . \qquad \text{(III.12)}$$

If we substitute into Eq. (III.12), the expression E_P[Eq. (III.10)] and assume $E_R >> \Gamma$ we obtain

$$D(E) = \left(\frac{2}{\Gamma} + \frac{i/2}{\sqrt{E_R(E_R - i\Gamma/2}} \right) (E_P - E) . \qquad \text{(III.13)}$$

Simplifying, we get

$$D(E) = \left(\frac{2}{\Gamma - \frac{i\Gamma^2}{4E_R}} \right) (E_P - E) . \qquad \text{(III.14)}$$

The residue of the pole is defined by

$$R = \lim_{E \to E_P} \frac{(E_P - E)}{D(E)} . \qquad \text{(III.15)}$$

Therefore we see that

$$R = \frac{\Gamma}{2} - \frac{i\Gamma^2}{8E_R} . \qquad \text{(III.16)}$$

The residue of the T-matrix is related to the coupling of the resonance. We may define the coupling such that $\Gamma_{total} = 2\Delta\chi$ (coupling). But the question is what momentum should we use in calculating the total width. For the coupling we used the residue of the pole, so one might think that the momentum at the pole should be used. On the other hand the momentum on the real axis tells us how much of the coupling is physically seen.

$$K = \frac{\Gamma/2}{E_R - E} + B. \tag{IV.1}$$

Here E is the total-center-of-mass energy, E_R is the pole position, $\Gamma/2$ is the coupling, and B is the background. T is given by

$$T = \frac{K}{1 - i\Delta K}, \tag{IV.2}$$

where Δ is the kinematic factor which we will take the same as in Appendix III:

$$\Delta = \sqrt{\frac{E}{E_R}}. \tag{IV.3}$$

Substituting Eq. (IV.1) into (IV.2), we get

$$T = \frac{1}{\left(\frac{\frac{E_R - E}{\Gamma/2}}{1 + \frac{B(E_R - E)}{\Gamma/2}} - i\sqrt{\frac{E}{E_R}} \right)}. \tag{IV.4}$$

If we assume $|B| << 1$, then

$$T = \frac{1}{\frac{E_R - E}{\Gamma/2} - \frac{B(E_R - E)^2}{\Gamma^2/4} - \frac{E}{E_R}}. \tag{IV.5}$$

We know that we will have a pole in T when we have a zero in D(E), the denominator of T. Let E_P be the value of E where D(E) is equal to zero:

$$D(E_P) = 0. \tag{IV.6}$$

Then by substitution of E_P into Eq. (IV.6), we obtain

$$\left(\frac{(E_R - E_P)}{\Gamma/2} - \frac{B(E_R - E_P)^2}{\Gamma^2/4} \right)^2 = -\frac{E_P}{E_R} \tag{IV.7}$$

or

$$-\frac{16B(E_R-E_P)^3}{\Gamma^3}+\frac{4(E_R-E_P)^2}{\Gamma^4}-\frac{(E_R-E_P)}{E_R}+1=0, \qquad \text{(IV.8)}$$

where we have dropped the factor of B^2/Γ^4. If we assume $E_R >> \Gamma >> |B|$ and $|B| << 1$, then a solution of Eq. (IV.8) is

$$E_P = E_R + \frac{\Gamma B}{2} - \frac{\Gamma^2}{8E_R} - \frac{i\Gamma}{2}\sqrt{1-\frac{\Gamma^2}{16E_R}}\,. \qquad \text{(IV.9)}$$

In this approximation we see, from Eq. (IV.9), that the real part of the pole position has been shifted by $\Gamma B/2$ from the normal Breit-Wigner pole (see Appendix IV) due to the presence of the background. We also should note that the shift can be either up or down in energy, depending on the sign of the background. For a narrow resonance with a small background the shift will be to first order in the real part of the pole position.

APPENDIX V

S-WAVE DOMINANCE OF THE ηN CROSS SECTION

In this appendix we estimate the minimum partial wave cross section for the $\pi^- p \to \eta n$ by using moments and the assumption of S-wave dominance around the 1520-MeV c.m. energy region.

If we assume that only S11, P11, D13, D15 and F15 waves contribute to the ηN channel and that they all have the same phase, we then will obtain the minimum amount of these waves necessary to generate the moments. From Ref. 16 we obtain the moment expressions:

$$C_0 = |S11|^2 + |P11|^2 + 2|D13|^2 + 3|D15|^2 + 3|F15|^2,$$
$$C_1 = 2|S11||P11| + 4|P11||D13| + 7.2|D13||F15| + 0.515|D15||F15|,$$
$$C_2 = 4|S11||D13| + 6|S11||D15| + 6|P11||F15| + 2|D13|^2 + 1.714|D13||F15| + 3.429|D15|^2 + 3.429|F15|^2,$$
$$C_3 = 6|S11||F15| + 6|P11||D15| + 4.8|D13||F15| + 3.2|D15||F15| . \qquad (V.1)$$

From our K-matrix fits to the S11 wave, we know that most of the cross section goes into S11 around 1520. Therefore we will assume S-wave dominance. Dropping all terms except those which have S-waves in them, we get for the moments:

$$C_0 = |S11|^2,$$
$$C_1 = 2|S11||P11|,$$
$$C_2 = 4|S11||D13| + 6|S11||D15|, \qquad (V.2)$$
$$C_3 = 6|S11||F15|.$$

We now can easily show that the ratio of the cross section of P11, D13, or D15, F15 to S11 can be written as

$$\frac{\sigma_{P11}}{\sigma_{S11}} = \frac{|P11|^2}{|S11|^2} = \left(\frac{C_1}{2C_0}\right)^2,$$
$$\frac{\sigma_{D13(only)}}{\sigma_{S11}} = \frac{2|D13|^2}{|S11|^2} = \frac{1}{2}\left(\frac{C_2}{2C_0}\right)^2, \qquad (V.3)$$
$$\frac{\sigma_{D15(only)}}{\sigma_{S11}} = \frac{3|D15|^2}{|S11|^2} = \frac{1}{3}\left(\frac{C_2}{2C_0}\right)^2,$$
$$\frac{\sigma_{F15}}{\sigma_{S11}} = \frac{3|F15|^2}{|S11|^2} = \frac{1}{3}\left(\frac{C_3}{2C_0}\right)^2.$$

A summary of these cross-section ratios taken from the moments of Lemoigne et al.[14] are shown in Table VII for 1520 to 1590 MeV. We conclude from Table VII and Fig. 9 that the S11 ηN is reasonably

predicted from our K-matrix fit and small (~ 5%) total contribution of higher waves (not permitted in our fit) to this channel could well describe the moments for $\pi^- p \to \eta N$.

Table I. Parameters of Breit-Wigner used in Watson final state factors equation (18).

Isobar, a	Mass, Er_a (pion masses)	Width, γ_a (dimensionless)	Orbital angular momentum, ℓ_a
Delta	8.83	0.40	1
Rho	5.464	0.20	1
Epsilon	6.0	0.8	0

Table II. Comparison of P11 solutions of Sec. 3.2 with two poles and three poles.

P11 solution with two poles		P11 solution with three poles	
χ^2 per deg. of freedom elastic + inelastic	1.47	χ^2 per deg. of freedom elastic + inelastic	1.62
χ^2 elastic	45	χ^2 elastic	58

Table III. K-matrix parameters of all waves, in sequence S, P, D, F.
[The parameters are defined in Eq. (25).]

Table IIIa

Wave	S11, CERN	S11, Saclay	S31, CERN	S31, Saclay
Energy range (MeV)	1310-1810	1310-1810	1310-1810	1310-1810
χ^2	88.7	57.2	136.4	141.7
Degrees of freedom	62	62	73	73
Channel 1	$N\pi$, L = 0	$N\pi$, L = 0	$N\pi$, L = 0	$N\pi$, L = 0
Channel 2	$N\epsilon$, L = 1	$N\epsilon$, L = 1	$\Delta\pi$, L = 2	$\Delta\pi$, L = 2
Channel 3	$N\rho_{1/2}$, L = 0	$N\rho_{1/2}$, L = 0	$N\rho_{1/2}$, L = 0	$N\rho_{1/2}$, L = 0
Channel 4	$N\eta$, L = 0	$N\eta$, L = 0	---	---
$\gamma_1^{1 \leftarrow \text{Pole}}$ $_{1 \leftarrow \text{Channel}}$	.345±.009	-.047±.020	1.786±.012	2.000±.013
$\gamma_2^{1}(^{\text{Pion}}_{\text{mass}})$	3.798±.035	3.235±.161	-4.932±.215	-5.784±.166
$\gamma_3^{1}(^{\text{Pion}}_{\text{mass}})$	1.351±.092	.531±.100	-2.802±.149	-2.852±.142
$\gamma_4^{1}(^{\text{Pion}}_{\text{mass}})$	-2.539±.022	-3.535±.037	---	---
$\gamma_1^{2 \leftarrow \text{Pole}}$ $_{1 \leftarrow \text{Channel}}$	3.431±.004	3.358±.002	---	---
$\gamma_2^{2}(^{\text{Pion}}_{\text{mass}})$	-1.676±.005	-2.273±.040	---	---
$\gamma_3^{2}(^{\text{Pion}}_{\text{mass}})$	2.329±.010	1.876±.050	---	---

Table IIIb

	S11, CERN	S11, Saclay	S31, CERN	S31, Saclay
$\gamma_4^2(\text{Pion mass})$	-1.688± .009	-2.209± .0216	---	---
Pole 1 (MeV)	1493± .6	1483± 2.4	1598± 2.9	1602± .4
Pole 2 (MeV)	1691± .06	1691± .2	---	---
C_{11}	30.62± .013	30.55± .023	19.30± .085	20.44± .033
C_{12}	-56.53± .189	-59.70± .690	-126.28± 2.370	-88.42± .675
C_{13}	-5.61± .117	-3.21± .074	3.54± .828	-22.64± .374
C_{14}	6.55± .094	.37± .062	---	---
C_{22}	157.27± 2.35	100.52± 1.970	-2046.18± 14.030	-2318.66± 5.574
C_{23}	66.43± .147	70.69± .469	-703.34± 3.162	-1346.85± 3.207
C_{24}	-64.08± .112	-63.96± .193	---	---
C_{33}	33.16± .169	37.44± 1.173	---	---
C_{34}	-19.27± .130	-12.34± 2.021	---	---
C_{44}	97.65± .271	98.18± .964	---	---
$B_{11}(\text{Pion mass})^{-1}$	-1.85± .003	-1.71± .002	-3.68± .010	-3.86± .002
$B_{12}(\text{Pion mass})^{-1}$	5.32± .017	5.73± .031	14.02± .114	10.76± .024

Table IIIc

	S11, CERN	S11, Saclay	S31, CERN	S31, Saclay
$B_{13}(\frac{Pion}{mass})^{-1}$	.34±.006	.46±.010	-.39±.059	2.14±.016
$B_{14}(\frac{Pion}{mass})^{-1}$	2.94±.011	3.97±.011	---	---
$B_{22}(\frac{Pion}{mass})^{-1}$	-12.14±.231	-7.49±.022	173.60±.976	280.0 ±.298
$B_{23}(\frac{Pion}{mass})^{-1}$	-4.63±.017	-4.23±.044	64.25±.233	120.29±.252
$B_{24}(\frac{Pion}{mass})^{-1}$	3.47±.011	3.61±.008	---	---
$B_{33}(\frac{Pion}{mass})^{-1}$	-5.31±.038	-4.29±.109	68.65±.940	109.29±.344
$B_{34}(\frac{Pion}{mass})^{-1}$	2.76±.032	2.67±.179	---	---
$B_{44}(\frac{Pion}{mass})^{-1}$	-3.55±.020	-2.76±.050	---	---
Partial width 1 (MeV)	1.216	.022	35.703	44.793
Partial width 2 (MeV)	43.738	30.799	33.096	46.878
Partial width 3 (MeV)	7.754	1.186	33.587	34.684
Partial width 4 (MeV)	12.255	0.000	---	---
Total width (MeV)	64.963	32.007	102.386	126.355
Partial width 1 (MeV)	139.976	134.071	---	---
Partial width 2 (MeV)	12.693	23.324	---	---

Table IIId

	S11, CERN	S11, Saclay
Partial width 3 (MeV)	21.215	13.768
Partial width 4 (MeV)	23.282	39.847
Total width (MeV)	197.166	211.009

Table IIIc

Wave	P11, CERN	P11, Saclay	P13, CERN	P13, Saclay
Energy range (MeV)	1310-2010	1310-2010	1520-2010	1520-2010
χ^2	152.6	160.6	117.6	89.1
Degrees of freedom	98	98	47	47
Channel 1	N π, L = 1	N π, L = 1	N π, L = 1	N π, L = 1
Channel 2	Δ π, L = 1	Δ π, L = 1	N $\rho_{1/2}$, L = 1	N $\rho_{1/2}$, L = 1
Channel 3	N ϵ, L = 0	N ϵ, L = 0	---	---
$\gamma^{1 \leftarrow \text{Pole}}_{\text{Channel}}$	4.919±.047	4.871±.014	2.497±.044	2.541±.039
$\gamma_2^{1}(^{\text{Pion}}_{\text{mass}})$	5.935±.135	6.386±.026	-7.465±.088	-7.506±.092
$\gamma_3^{1}(^{\text{Pion}}_{\text{mass}})$	-2.347±.111	-1.848±.039	---	---
$\gamma_1^{2}(^{\text{Pion}}_{\text{mass}})$	5.838±.192	5.277±.015	---	---
$\gamma_2^{2}(^{\text{Pion}}_{\text{mass}})$	-4.831±.155	-4.176±.018	---	---
$\gamma_3^{2}(^{\text{Pion}}_{\text{mass}})$	4.915±.170	4.592±.010	---	---
Pole 1 (MeV)	1477±1.5	1476±1.2	1809±5.4	1809±4.9
Pole 2 (MeV)	1870±4.9	1869±.7	---	---

Table IIIf

	P11, CERN	P11, Saclay	P13, CERN	P13, Saclay
C_{11}	-8.61± .500	-12.28± .730	-8.78± .130	-12.82± .090
C_{12}	22.85± 4.903	14.47± .242	-8.26± .106	-2.88± .405
C_{12}	24.38± 4.440	15.54± .128	---	---
C_{22}	144.54± 2.038	93.08± .144	-179.10± 1.593	-219.70± 1.038
C_{23}	19.28± .146	46.34± .491	---	---
C_{33}	-6.92± 3.168	42.92± .930	---	---
$B_{11}(\frac{\text{Pion}}{\text{mass}})^{-1}$	-.18± .047	.43± .056	.17± .001	.49± .005
$B_{12}(\frac{\text{Pion}}{\text{mass}})^{-1}$	-.40± .402	-.35± .021	1.02± .033	.58± .003
$B_{13}(\frac{\text{Pion}}{\text{mass}})^{-1}$	-3.48± .376	-2.74± .024	---	---
$B_{22}(\frac{\text{Pion}}{\text{mass}})^{-1}$	-9.02± .154	-.82± .056	14.81± .026	17.90± .031
$B_{23}(\frac{\text{Pion}}{\text{mass}})^{-1}$	-.21± .047	.81± .035	---	---
$B_{33}(\frac{\text{Pion}}{\text{mass}})^{1}$	.88± .273	-.89± .044	---	---
Partial width 1 (MeV)	200.045	196.060	71.998	74.574
Partial Width 2 (MeV)	66.999	77.285	235.844	238.961
Partial Width 3 (MeV)	27.561	17.091	---	---

Table IIIg

	P11, CERN	P11, Saclay	P13, CERN	P13, Saclay
Total width (MeV)	294.605	290.435	307.842	313.525
Partial width 1 (MeV)	407.369	332.702	---	---
Partial width 2 (MeV)	171.665	128.176	---	---
Partial width 3 (MeV)	182.936	159.541	---	---
Total width (MeV)	761.971	620.419	---	---

sure that the asymmetries in these two solvents are due almost exclusively to hot reactions. Independent studies of this type[27] verify that the asymmetries observed in methanol, hexane, and heptane are due only to hot chemistry.

Asymmetries in hydrocarbons tend to increase with the number of hydrogen atoms per molecule, except when the compound is unsaturated, in which case the H atoms are presumably more tightly bound. Note the marked difference between hexene and cyclohexane, which differ only in bond structure, and the exceptionally low asymmetry in benzene, where the H atoms are particularly tightly bound by the "resonance" effect[28]. The high asymmetry observed in glycerol and in halide-substitued forms of methane may be due to thermal reactions.

The results obtained for muonium hot chemistry may be compared and combined with analogous results from hot tritium (T) chemistry[12,17], in which it is more difficult to tell "hot" from "cold" reaction products, but where it is possible to distinguish between different diamagnetic products (e.g., TH vs. THO in hot reactions with water).

We have not yet seriously attempted to develop the potentialities of this technique for studying hot atom chemistry; however, it seems clear that the field should benefit broadly from this technique[29].

Table III i

	D13, CERN	D13, Saclay	D33, CERN	D33, Saclay
$\gamma_2^{2,\text{Pion}}_{(\text{mass})}$	-9.624± .211	-8.989± .176	---	---
$\gamma_3^{2,\text{Pion}}_{(\text{mass})}$	-3.859± .087	-3.498± .239	---	---
$\gamma_4^{2,\text{Pion}}_{(\text{mass})}$	19.339± .255	20.764± .563	---	---
$\gamma_5^{2,\text{Pion}}_{(\text{mass})}$	-11.453± .920	-13.464± .375	---	---
$\gamma_1^{3,\text{Pion}}_{(\text{mass})}$	2.122± .028	1.679± .082	---	---
$\gamma_2^{3,\text{Pion}}_{(\text{mass})}$	-2.171± .156	-3.354± .381	---	---
$\gamma_3^{3,\text{Pion}}_{(\text{mass})}$	-7.734± .006	-8.463± .134	---	---
$\gamma_4^{3,\text{Pion}}_{(\text{mass})}$	9.484± .247	11.548± .262	---	---
$\gamma_5^{3,\text{Pion}}_{(\text{mass})}$	11.465± .399	13.381± .139	---	---
Pole 1 (MeV)	1508± 1.0	1510± 1.0	1697± 6.1	1704± .9
Pole 2 (MeV)	1878± .6	1908± 6.5	---	---
Pole 3 (MeV)	2218± 3.9	2261± 7.8	---	---
C_{11}	-11.18 ± .143	-10.52 ± .167	51.26± .033	51.33± .076
C_{12}	-17.82 ± .150	-16.38 ± .433	-8.76± 1.640	-5.23± .065
C_{13}	-6.45 ± .215	-8.62 ± .678	-65.73± .078	-65.39± .055

Table III j

	D13, CERN	D13, Saclay	D33, CERN	D33, Saclay
C_{14}	53.20±.634	55.29±.806	---	---
C_{15}	-35.10±.495	35.10±.663	---	---
C_{22}	-60.00±2.964	-67.08±5.070	545.88±.196	545.94±.798
C_{23}	-36.74±.658	-36.20±3.261	-32.61±.710	-31.98±.263
C_{24}	162.92±2.459	179.76±2.486	---	---
C_{25}	20.48±1.102	47.78±5.253	---	---
C_{33}	-59.50±4.885	-44.28±5.015	204.29±1.036	208.41±.609
C_{34}	85.85±.117	89.84±5.895	---	---
C_{35}	-91.71±2.298	-80.34±4.699	---	---
C_{44}	-60.93±3.446	-65.51±1.842	---	---
C_{45}	2.55±5.885	1.881±6.090	---	---
C_{55}	-293.10±8.500	-315.52±6.746	---	---
$B_{11}(\frac{\text{Pion}}{\text{mass}})^{-1}$	.65±.005	.71±.011	-4.85±.025	-4.88±.008
$B_{12}(\frac{\text{Pion}}{\text{mass}})^{-1}$	.06±.017	.24±.014	-.95±.182	-2.33±.008
$B_{13}(\frac{\text{Pion}}{\text{mass}})^{-1}$	.58±.012	.82±.047	6.25±.074	6.18±.003

Table IIIk

	D13, CERN	D13, Saclay	D33, CERN	D33, Saclay
$B_{14}(\frac{Pion}{mass})^{-1}$	-2.13±.047	-2.45±.041	---	---
$B_{15}(\frac{Pion}{mass})^{-1}$	.23±.014	.41±.013	---	---
$B_{22}(\frac{Pion}{mass})^{-1}$	3.70±.152	4.88±.332	-51.18±.268	-52.06±.080
$B_{23}(\frac{Pion}{mass})^{-1}$	.75±.064	1.07±.421		
$B_{24}(\frac{Pion}{mass})^{-1}$	-3.32±.126	-5.52±.238	---	---
$B_{25}(\frac{Pion}{mass})^{-1}$	-1.86±.192	-2.68±.184	---	---
$B_{33}(\frac{Pion}{mass})^{-1}$	1.12±.350	-.02±.245	-16.25±.238	-16.59±.057
$B_{34}(\frac{Pion}{mass})^{-1}$	-.35±.090	-.95±.370	---	---
$B_{35}(\frac{Pion}{mass})^{-1}$	-.62±.225	-.89±.259	---	---
$B_{44}(\frac{Pion}{mass})^{-1}$	-15.30±.474	-15.88±.421	---	---
$B_{45}(\frac{Pion}{mass})^{-1}$	15.15±.058	15.34±.055	---	---
$B_{55}(\frac{Pion}{mass})^{-1}$	-7.98±1.29	-9.98±1.100	---	---
Partial width 1 (MeV)	69.150	70.211	33.127	42.142
Partial width 2 (MeV)	32.126	33.114	201.740	273.255
Partial width 2 (MeV)	16.021	15.967	72.634	75.471

Table III 1

	D13, CERN	D13, Saclay	D33, CERN	D33, Saclay
Partial width 4 (MeV)	.002	.022	---	---
Partial width 5 (MeV)	20.633	25.116	---	---
Total width (MeV)	137.932	144.420	307.502	390.868
Partial width 1 (MeV)	160.157	148.584	---	---
Partial width 2 (MeV)	810.063	725.494	---	---
Partial width 3 (MeV)	105.730	92.888	---	---
Partial width 4 (MeV)	2322.352	2800.493	---	---
Partial width 5 (MeV)	652.554	967.023	---	---
Total width (MeV)	4050.857	4734.482	---	---
Partial width 1 (MeV)	55.182	35.100	---	---
Partial width 2 (MeV)	51.273	124.672	---	---
Partial width 3 (MeV)	642.319	789.966	---	---
Partial width 4 (MeV)	815.626	1246.676	---	---
Partial width 5 (MeV)	1097.227	1551.926	---	---
Total width (MeV)	2661.627	3748.340	---	---

Table III m

Wave	D15, CERN	D15, Saclay	F15, CERN	F15, Saclay
Energy range (MeV)	1585–1810	1585–1810	1585–1810	1585–1810
χ^2	58.7	69.6	44.2	30.9
Degrees of freedom	20	20	31	31
Channel 1	$N\pi\ \ell=2$	$N\pi\ \ell\ \ 2$	$N\pi\ \ \ell\ \ 3$	$N\pi\ \ell\ \ 3$
Channel 2	$\Delta\pi\ \ell=2$	$\Delta\pi\ \ell\ \cdot\ 2$	$\Delta\pi\ \ \ell\ =1$	$\Delta\pi\ \ell\ \ 1$
Channel 3	---	---	$N\rho_{3/2}\ \ell=1$	$N\rho_{3/2}\ \ell=1$
Channel 4	---	---	$N\epsilon\ \ \ell=2$	$N\epsilon\ \ \ell=2$
γ_1^1 ← Pole γ_1 ← Channel	2.890±.047	2.840±.055	4.427±.035	4.362±.034
γ_2^1(Pion mass)	-6.265±.154	-6.064±.163	1.000±.053	1.147±.053
γ_3^1(Pion mass)	---	---	5.007±.205	4.843±.200
γ_4^1(Pion mass)	---	---	2.684±.186	2.588±.182
Pole 1 (MeV)	1684±3.3	1683±3.2	1684±.8	1682±.8
C_{11}	-.59 ±.620	-1.02 ±.607	4.71 ±.338	3.64 ±.261
C_{12}	-5.22 ±1.834	.93 ±1.841	-8.34 ±.126	-7.86 ±1.273

Table IIIa

	D15, CERN	D15, Saclay	F15, CERN	F15, Saclay
C_{13}	---	---	-1.49±1.055	-1.00±1.045
C_{14}	---	---	-.15±1.911	-1.80±1.952
C_{22}	6.22±8.612	-1.54±8.808	-27.00±5.100	-23.52±4.662
C_{23}	---	---	53.41±2.753	50.26±2.131
C_{24}	---	---	9.26±2.881	7.30±2.867
C_{33}	---	---	-40.67±5.886	-40.31±6.029
C_{34}	---	---	-39.64±8.290	-40.08±8.032
C_{44}	---	---	15.03±10.089	14.54±10.223
Partial width 1	66.192	63.815	83.458	80.647
Partial width 2	95.488	89.133	5.177	6.772
Partial width 3	---	---	53.153	49.731
Partial width 4	---	---	15.293	14.154
Total width	161.680	152.948	157.080	151.305

Table III o

Wave	F35, CERN	F35, Saclay	F37, CERN	F37, Saclay
Energy range (MeV)	1730–2010	1730–2010	1770–2010	1770–2010
χ^2	26.5	20.7	23.0	9.5
Degrees of freedom	34	34	23	23
Channel 1	N π, L = 3	N π, L = 3	N π, L = 3	N π, L = 3
Channel 2	Δ π, L = 3	Δ π, L = 3	Δ π, L = 3	Δ π, L = 3
Channel 3	N $\rho_{3/2}$, L = 1	N $\rho_{3/2}$, L = 1	N $\rho_{3/2}$, L 3	N $\rho_{3/2}$, L = 3
Channel 4	---	---	$\Delta\rho$, L 1	$\Delta\rho$, L 1
γ^{1-}_{1-} Pole Channel	4.282±.263	4.179±1.691	3.794±.030	3.513±.005
γ^{1}_{2}(Pion mass)	2.938±5.451	5.178±1.509	9.019±.084	6.099±.142
γ^{1}_{3}(Pion mass)	-18.321±4.391	-15.666±7.688	-4.502±.101	-3.296±.128
γ^{1}_{4}(Pion mass)	---	---	7.238±.183	8.041±.033
Pole 1 (MeV)	2169±60.5	2136±125.9	1941±1.2	1921±.8
C_{11}	-4.16 ±.473	-3.80 ±3.319	2.82 ±.073	3.08 ±.286
C_{12}	-3.79 ±7.217	-6.42 ±6.268	2.74 ±.714	6.59 ±.919

Table III p

	F35, CERN	F35, Saclay	F37, CERN	F37, Saclay
C_{13}	6.68±3.579	5.97±13.788	3.27±1.50	8.74±.400
C_{14}	---	---	-15.191±.555	-17.07±.670
C_{22}	-169.24±28.034	-142.68±50.356	173.02±7.348	156.74±4.310
C_{23}	-57.69±53.152	-31.04±2.096	-56.51±3.496	39.39±3.748
C_{24}	---	---	-115.81±3.850	-78.08±.922
C_{33}	-127.87±48.838	101.78±65.735	-221.14±7.150	-308.52±5.43
C_{34}	---	---	154.91±8.074	190.03±.890
C_{44}	---	---	-51.17±7.081	-23.62±4.058
Partial width 1 (MeV)	177.921	164.775	108.736	90.432
Partial width 2 (MeV)	46.503	135.129	234.350	98.772
Partial width 3 (MeV)	3176.717	2245.710	34.511	15.721
Partial width 4 (MeV)	---	---	112.206	137.436
Total width (MeV)	3401.141	2545.615	489.803	342.361

Table IV. T-matrix poles and residues for all waves in sequence S, P, D, F. (Poles and partial widths (residues) are in MeV).

Table IVa

S11 CERN, First Pole

Real = 1503.2 ± .8 / Twice Imag = 64.8 ± 1.8

	$\Gamma_{(N\pi)}$	$\Gamma_{[N\epsilon(P)]}$	$\Gamma_{[N\rho_{1/2}(S)]}$	$\Gamma_{[N\eta(S)]}$	$\Gamma_{(total)}$	
Real	7.2	23.0 +	6.5 +	2.3 +	38.9	Real
Imag	-5.8i	35.4i	.2i	9.7i	39.5i	Imag
Mod	|9.2|	|42.2|	|6.5|	|10.0|	|68.0|[a]	Mod

S11 Saclay, First Pole

Real = 1491.4 ± 2.9 / Twice Imag = 57.5 ± 3.3

	$\Gamma_{(N\pi)}$	$\Gamma_{[N\epsilon(P)]}$	$\Gamma_{[N\rho_{1/2}(S)]}$	$\Gamma_{[N\eta(S)]}$	$\Gamma_{(total)}$	
Real	.8	11.7 +	.4 +	-.8 +	12.0	Real
Imag	-13.4i	28.1i	1.4i	14.1i	30.2i	Imag
Mod	|13.4|	|30.5|	|1.4|	|14.1|	|59.4|[a]	Mod

S11 CERN, Second Pole

Real = 1652.4 ± .2 / Twice Imag = 100.3 ± .8

	$\Gamma_{(N\pi)}$	$\Gamma_{(N\epsilon(P)]}$	$\Gamma_{[N\rho_{1/2}(S)]}$	$\Gamma_{[N\eta(S)]}$	$\Gamma_{(total}$	
Real	26.1	-2.3 -	-2.6 +	4.7 -	25.9	Real
Imag	-36.8i	-3.7i	-8.9i	-31.9i	-81.2i	Imag
Mod	|45.1|	|4.4|	|9.2|	|32.3|	|90.9|	Mod

[a] Modulus of Γ (total) is sum of moduli of Γ_i.

Table IVb

S11 Saclay, Second Pole

Real 164.4 ± 0.4 Twice Imag 103.6 ± 2.1

	$\Gamma_{(N\pi)}$	$\Gamma_{\lvert N\epsilon(P)\rvert}$	$\Gamma_{[N\rho_{1/2}(S)]}$	$\Gamma_{[N\eta(S)]}$	$\Gamma_{(total)}$	
Real	18.8	0.4	-2.7	8.4	24.8	Real
Imag	-41.2i	-7.9i	-5.0i	-31.0i	-85.1i	Imag
Mod	|45.3	|7.9|	|5.7|	|32.1	91.0 [a]	Mod

S31 CERN, Pole

Real 1600.3 ± 4.8 Twice Imag 79.2 ± 10.4

	$\Gamma_{(N\pi)}$	$\Gamma_{\lvert\Delta\pi(D)\rvert}$	$\Gamma_{[N\rho_{1/2}(S)]}$	$\Gamma_{(total)}$	
Real	-3.2	22.0	-5.3	13.4	Real
Imag	-19.5i	15.8i	101.9i	98.2i	Imag
Mod	19.8	27.1	102.0	148.9 [a]	Mod

S31 Saclay

Real 1602.4 ± 3.9 Twice Imag 74.1 ± 6.1

	$\Gamma_{(N\pi)}$	$\Gamma_{[\Delta\pi(D)]}$	$\Gamma_{[N\rho_{1/2}(S)]}$	$\Gamma_{(total)}$	
Real	-4.2	24.5	-56.6	-36.3	Real
Imag	-19.2i	7.0i	56.4i	44.2i	Imag
Mod	|19.7	|25.5|	|79.9|	125.1 [a]	Mod

[a] Modulus of Γ (total) is sum of moduli of Γ_i.

Table IV c

P11 CERN, First Pole

Real = 1384.6 ± 2.8 / Twice Imag 234.7 ± 4.3

	$\Gamma_{(N\pi)}$	$\Gamma_{[\Delta\pi(P)]}$	$\Gamma_{[N\epsilon(S)]}$	$\Gamma_{(total)}$	
Real	36.0	21.0 $^{+}$	5.1 $^{-}$	62.1	Real
Imag	-109.2i	-25.5i	-5.1i	-139.9i	Imag
Mod	|115.0|	|33.0|	|7.2|	|155.2| [a]	Mod

P11 Saclay, First Pole

Real = 1391.0 ± 0.5 / Twice Imag = 206.3 ± 1.8

	$\Gamma_{(N\pi)}$	$\Gamma_{[\Delta\pi(P)]}$	$\Gamma_{[N\epsilon(S)]}$	$\Gamma_{(total)}$	
Real	29.5	29.5 $^{+}$	2.0 $^{-}$	61.0	Real
Imag	-85.4i	-30.9i	0.6i	-115.7i	Imag
Mod	|90.3|	|42.8|	|2.1|	|135.1| [a]	Mod

P11 CERN, Second Pole

Real = 1724.5 ± 5.5 / Twice Imag = 282.6 ± 8.2

	$\Gamma_{(N\pi)}$	$\Gamma_{[\Delta\pi(P)]}$	$\Gamma_{[N\epsilon(S)]}$	$\Gamma_{(total)}$	
Real	-39.4	46.6 $^{-}$	31.0 $^{+}$	38.1	Real
Imag	-115.0i	5.3i	-55.9i	-165.6i	Imag
Mod	|121.3|	|46.9|	|63.9|	|232.3| [a]	Mod

[a] Modulus of $\Gamma_{(total)}$ is sum of moduli of Γ_i.

Table IV d

P11 Saclay, Second Pole

Real = 1744.1 ± 1.0 / Twice Imag = 293.7 ± 5.0

	$\Gamma_{(N\pi)}$	$\Gamma_{[\Delta\pi(P)]}$	$\Gamma_{[N\epsilon(S)]}$	$\Gamma_{(total)}$	
Real	-22.6	38.4	60.5	76	Real
Imag	-126.3i	3.7i	-57.6i	-180.2i	Imag
Mod	| 128.3 |	| 38.6 |	| 83.5 |	250.4 [a]	Mod

P13 CERN Pole

Real = 1728.2 ± 2.3 / Twice Imag = 150.3 ± 5.6

	$\Gamma_{(N\pi)}$	$\Gamma_{[N\rho_{1/2}(P)]}$	$\Gamma_{(total)}$	
Real	0.5	42.3	42.8	Real
Imag	-25.3i	-72.7i	-97.9i	Imag
Mod	| 25.3 |	| 84.1 |	| 109.3 | [a]	Mod

P13 Saclay Pole

Real = 1727.7 ± 2.1 / Twice Imag = 156.9 ± 4.9

	$\Gamma_{(N\pi)}$	$\Gamma_{[N\rho_{1/2}(P)]}$	$\Gamma_{(total)}$	
Real	1.5	38.5	40.0	Real
Imag	-26.0i	-69.8i	-95.8i	Imag
Mod	| 26.0 |	| 79.7 |	105.8 [a]	Mod

[a] Modulus of $\Gamma_{(total)}$ is sum of moduli of Γ_i.

Table IV e

D13 CERN, First Pole

	Real = 1514.6 ± 2.1			Twice Imag = 142.1 ± 5.4			
	$\Gamma_{(N\pi)}$	$\Gamma_{[\Delta\pi(S)]}$	$\Gamma_{[N\rho_{3/2}(S)]}$	$\Gamma_{[N\epsilon(P)]}$	$\Gamma_{[\Delta\pi(D)]}$	$\Gamma_{(total)}$	
Real	88.1	5.1 $^{-}$	33.7 $^{+}$	-3.4 $^{-}$	3.2	126.7	Real
Imag	12.5i	35.9i	5.7i	0.3i	13.5i	67.9i	Imag
Mod	| 89.0 |	| 36.3 |	| 34.2 |	| 3.4 |	| 13.8 |	| 176.7 |[a]	Mod

D13 Saclay, First Pole

	Real = 1514.9 ± 4.8			Twice Imag = 148.9 ± 6.4			
	$\Gamma_{(N\pi)}$	$\Gamma_{[\Delta\pi(S)]}$	$\Gamma_{[N\rho_{3/2}(S)]}$	$\Gamma_{[N\epsilon(P)]}$	$\Gamma_{[\Delta\pi(D)]}$	$\Gamma_{(total)}$	
Real	91.3	7.9 $^{-}$	35.6 $^{+}$	-4.0 $^{-}$	3.3 $^{-}$	134.2	Real
Imag	10.4i	40.1i	5.3i	0.3i	14.3i	70.5i	Imag
Mod	| 91.9 |	| 40.9 |	| 36.0 |	| 4.0 |	| 14.7 |	| 187.5 |[a]	Mod

D13 CERN, Second Pole

	Real = 1646.9 ± 6.5			Twice Imag = 116.6 ± 5.4			
	$\Gamma_{(N\pi)}$	$\Gamma_{[\Delta\pi(S)]}$	$\Gamma_{[N\rho_{3/2}(S)]}$	$\Gamma_{[N\epsilon(P)]}$	$\Gamma_{[\Delta\pi(D)]}$	$\Gamma_{(total)}$	
Real	5.3	-8.0 $^{+}$	-.7 $^{-}$	-56.9 $^{-}$	0.3 $^{-}$	-60.0	Real
Imag	-14.9i	-22.2i	3.6i	-31.7i	-2.4i	-67.5i	Imag
Mod	| 15.8 |	| 23.6 |	| 3.7 |	| 65.1 |	| 2.4 |	| 110.7 |[a]	Mod

[a] Modulus of $\Gamma_{(total)}$ is sum of moduli of Γ_i.

Table IV f

D13 Saclay, Second Pole

	Real = 1650.4 ± 12.4			Twice Imag = 125.4 ± 0.7			
	$\Gamma_{(N\pi)}$	$\Gamma_{[\Delta\pi(S)]}$	$\Gamma_{[N\rho_{3/2}(S)]}$	$\Gamma_{[N\epsilon(P)]}$	$\Gamma_{[\Delta\pi(D)]}$	$\Gamma_{(total)}$	
Real	5.0	-9.2 $^{+}$	-.5 $^{-}$	-63.3 $^{-}$	0.2 $^{-}$	-67.8	Real
Imag	-12.6i	-23.1i	4.1i	-39.8i	-1.3i	-72.8i	Imag
Mod	| 13.6 |	| 24.9 |	| 4.1 |	| 74.8 |	| 1.3 |	| 118.6 | [a]	Mod

D13 CERN, Third Pole

	Real = 1971.0 ± 11.5			Twice Imag = 452.1 ± 37.4			
	$\Gamma_{(N\pi)}$	$\Gamma_{[\Delta\pi(S)]}$	$\Gamma_{[N\rho_{3/2}(S)]}$	$\Gamma_{[N\epsilon(P)]}$	$\Gamma_{[\Delta\pi(D)]}$	$\Gamma_{(total)}$	
Real	-1.9	-48.0 $^{+}$	110.6 $^{-}$	-2.0 $^{+}$	8.3 $^{+}$	67.0	Real
Imag	-87.2i	51.0i	-177.9i	1.3i	-27.4i	-240.3i	Imag
Mod	| 87.2 |	| 70.1 |	| 209.5 |	| 2.4 |	| 28.6 |	| 397.8 | [a]	Mod

D13 Saclay, Third Pole

	Real = 1970.7 ± 32.0			Twice Imag = 401.8 ± 52.4			
	$\Gamma_{(N\pi)}$	$\Gamma_{[\Delta\pi(S)]}$	$\Gamma_{[N\rho_{3/2}(S)]}$	$\Gamma_{[N\epsilon(P)]}$	$\Gamma_{[\Delta\pi(D)]}$	$\Gamma_{(total)}$	
Real	14.1	-48.3 $^{+}$	82.7 $^{-}$	-1.0 $^{+}$	0.6 $^{+}$	48.2	Real
Imag	-54.8i	47.3i	-170.2i	0.4i	-25.9i	-203.1i	Imag
Mod	| 56.6 |	| 67.6 |	| 189.2 |	| 1.1 |	| 25.9 |	| 340.3 | [a]	Mod

[a] Modulus of $\Gamma_{(total)}$ is sum of moduli of Γ_i.

Table IV g

D33 CERN Pole

Real = 1656.7 ± 5.3 / Twice Imag = 109.3 ± 2.3

	$\Gamma_{(N\pi)}$	$\Gamma_{[\Delta\pi(S)]}$	$\Gamma_{[N\rho_{3/2}(S)]}$	$\Gamma_{(total)}$	
Real	6.9	-6.6^{+}	35.9^{+}	36.2	Real
Imag	-3.4i	-45.1i	7.5i	-40.9i	Imag
Mod	| 7.7 |	| 45.5 |	| 36.6 |	| 89.8 |[a]	Mod

D33 Saclay Pole

Real 1654.4 ± 1.4 / Twice Imag = 117.5 ± 2.4

	$\Gamma_{(N\pi)}$	$\Gamma_{[\Delta\pi(S)]}$	$\Gamma_{[N\rho_{3/2}(S)]}$	$\Gamma_{(total)}$	
Real	6.9	-8.9^{+}	36.0^{+}	34.0	Real
Imag	-4.2i	-49.3i	8.5i	-44.9i	Imag
Mod	| 8.1 |	| 50.1 |	| 37.0 |	| 95.1 |	Mod

D15 CERN Pole

Real = 1665.7 ± 2.8 / Twice Imag = 159.0 ± 11.1

	$\Gamma_{(N\pi)}$	$\Gamma_{[\Delta\pi(D)]}$	$\Gamma_{(total)}$	
Real	67.7	91.0^{-}	158.8	Real
Imag	-13.8i	-10.4i	-24.2i	Imag
Mod	| 69.1 |	| 91.6 |	160.7 |[a]	Mod

[a] Modulus of $\Gamma_{(total)}$ is sum of moduli of Γ_i.

Table IV h

D15 Saclay Pole

Real = 1662.1 ± 2.2 / Twice Imag = 139.7 ± 9.2

	$\Gamma_{(N\pi)}$	$\Gamma_{[\Delta\pi(D)]}$	$\Gamma_{(total)}$	
Real	55.8	71.2 $^{-}$	127.0	Real
Imag	-18.2i	-21.2i	-39.4i	Imag
Mod	| 58.7 |	| 74.3 |	| 133.0 |[a]	Mod

F15 CERN Pole

Real = 1672.0 ± 2.4 / Twice Imag = 154.6 ± 5.2

	$\Gamma_{(N\pi)}$	$\Gamma_{[\Delta\pi(P)]}$	$\Gamma_{[N\rho_{3/2}(P)]}$	$\Gamma_{[N\epsilon(D)]}$	$\Gamma_{(total)}$	
Real	99.3	5.3 $^{+}$	32.5 $^{+}$	14.5 $^{+}$	151.6	Real
Imag	-17.1i	10.6i	-27.0i	-15.7i	-49.1i	Imag
Mod	| 100.7 |	| 11.9 |	| 42.2 |	| 21.4 |	| 176.2 |[a]	Mod

F15 Saclay Pole

Real = 1668.6 ± 2.0 / Twice Imag = 145.0 ± 4.8

	$\Gamma_{(N\pi)}$	$\Gamma_{[\Delta\pi(P)]}$	$\Gamma_{[N\rho_{3/2}(P)]}$	$\Gamma_{[N\epsilon(D)]}$	$\Gamma_{(total)}$	
Real	88.7	7.4 $^{+}$	29.9 $^{+}$	11.7 $^{+}$	137.6	Real
Imag	-20.4i	9.2i	-24.9i	-14.9i	-51.0i	Imag
Mod	| 91.0 |	| 11.8 |	| 38.9 |	| 18.9 |	| 160.6 |	Mod

[a]Modulus of $\Gamma_{(total)}$ is sum of moduli of Γ_i.

Table IV i

F35 CERN Pole

Real = 1624.1 ± 7.5 / Twice Imag = 282.1 ± 25.6

	$\Gamma_{(N\pi)}$	$\Gamma_{[\Delta\pi(F)]}$	$\Gamma_{[N\rho_{3/2}(P)]}$	$\Gamma_{(total)}$	
Real	36.3	19.1 $^{+}$	-20.3 $^{-}$	35.1	Real
Imag	-25.5i	-17.7i	-104.7i	-148.0i	Imag
Mod	| 44.3 |	| 26.1 |	| 106.7 |	| 177.1 |^{a}	Mod

F35 Saclay Pole

Real = 1831.9 ± 20.7 / Twice Imag = 277.5 ± 34.9

	$\Gamma_{(N\pi)}$	$\Gamma_{[\Delta\pi(F)]}$	$\Gamma_{[N\rho_{3/2}(P)]}$	$\Gamma_{(total)}$	
Real	36.2	15.7 $^{+}$	-17.1 $^{-}$	34.8	Real
Imag	-24.8i	-19.2i	-107.7i	-151.7i	Imag
Mod	| 43.9 |	| 24.8 |	| 109.0 |	| 177.8 |^{a}	Mod

F37 CERN Pole

Real = 1866.1 ± 5.8 / Twice Imag = 254.9 ± 21.4

	$\Gamma_{(N\pi)}$	$\Gamma_{[\Delta\pi(F)]}$	$\Gamma_{[N\rho_{3/2}(F)]}$	$\Gamma_{[\Delta\rho(P)]}$	$\Gamma_{(total)}$	
Real	78.2	12.0 $^{+}$	-34.9 $^{+}$	51.8 $^{+}$	107.1	Real
Imag	23.0i	54.7i	22.4i	-84.2i	15.9i	Imag
Mod	| 81.6 |	| 56.0 |	| 41.4 |	| 98.8 |	| 277.8 |^{a}	Mod

^{a}Modulus of $\Gamma_{(total)}$ is sum of moduli of Γ_i.

Table IV j

F37 Saclay Pole

Real = 1876.8 ± 6.2 Twice Imag = 297.8 ± 30.2

	$\Gamma_{(N\pi)}$	$\Gamma_{[\Delta\pi(F)]}$	$\Gamma_{[N\rho_{3/2}(F)]}$	$\Gamma_{[\Delta\rho(P)]}$	$\Gamma_{(total)}$	
Real	48.5	92.3 $^{+}$	-9.1 $^{+}$	58.0 $^{+}$	189.8	Real
Imag	-37.1i	26.0i	50.0i	-29.2i	9.8i	Imag
Mod	| 61.1 |	| 96.0 |	| 51.0 |	| 64.9 |	| 272.8 | [a]	Mod

[a] Modulus of $\Gamma_{(total)}$ is sum of moduli of Γ_i.

Table V. Comparison of parameters of K-matrix, T-matrix, and Breit-Wigner refit, all in MeV.

Table V a

2 Channel, Small Background, D15 CERN(EPSA)+Nππ

	Origin \ Parameter		Mass	$\Gamma_{(total)}$	$\Gamma_{(N\pi)}$	$\Gamma_{[\Delta\pi(D)]}$	
K-matrix	K-matrix pole from Table III	Real	1684	161	66	95	Real
	T-matrix pole[a] from Table IV	Real	1666	159	68	91	Real
		Imag	$\frac{-159i}{2}$	-24i	-14i	-10i	Imag
		Mod		|161|	|69|	|92|	Mod
U(UB+BW)	Unitarized (UB+BW) BW parameter	Real	1692	176	71	105	Real
UB+BW	Unitarized (UB+BW) BW pole[a]	Real	1666	156	68	88	Real
		Imag	$\frac{-158i}{2}$	-24i	-12i	-11i	Imag
		Mod		|158|	|69|	|89|	Mod
	UB+BW BW parameter	Real	1683	167	68	99	Real
	UB+BW BW pole[a]	Real	1659	134	57	77	Real
		Imag	$\frac{-150i}{2}$	-45i	-22i	-23i	Imag
		Mod		|141|	|61|	|80|	Mod

D15 CERN (EPSA) Only

	Origin \ Parameter		Mass	$\Gamma_{(total)}$	$\Gamma_{(N\pi)}$	$\Gamma_{[\Delta\pi(D)]}$	
K-matrix	K-matrix pole	Real	1682	156	64	92	Real
	T-matrix pole[a]	Real	1660	125	54	71	Real
		Imag	$\frac{-140i}{2}$	-43i	-20i	-23i	Imag
		Mod		|133|	|58|	|75|	Mod
UB+BW	UB+BW BW parameter	Real	1682	153	63	90	Real
	UB+BW BW pole[a]	Real	1661		55		Real
		Imag	$\frac{-140i}{2}$		-18i		Imag
		Mod			|58|		Mod

[a] T-matrix pole has complex position and p rtial width (Γ_i). Modulus of $\Gamma_{(total)}$ is the sum of the moduli of Γ_i.

Table V b

2 Channel, Small Background, D15 Saclay(EPSA)+Nππ

	Origin \ Parameter		Mass	$\Gamma_{(total)}$	$\Gamma_{(N\pi)}$	$\Gamma_{[\Delta\pi(D)]}$	
K-matrix	K-matrix pole from Table III	Real	1683	153	64	89	Real
K-matrix	T-matrix	Real	1662	127	56	71	Real
K-matrix	pole[a]	Imag	$\frac{-140i}{2}$	-39i	-18i	-21i	Imag
K-matrix	from Table IV	Mod		|133|	|59|	|74|	Mod
U(UB+BW)	Unitarized (UB+BW) BW parameter	Real	1684	153	64	89	Real
U(UB+BW)	Unitarized	Real	1663	130	56	74	Real
U(UB+BW)	(UB+BW)	Imag	$\frac{-140i}{2}$	-36i	-18i	-18i	Imag
U(UB+BW)	BW pole[a]	Mod		|135|	|59|	|76|	Mod
UB+BW	UB+BW BW parameter	Real	1684	153	64	89	Real
UB+BW	UB+BW	Real	1662	127	55	71	Real
UB+BW		Imag	$\frac{-140i}{2}$	-40i	-18i	-22i	Imag
UB+BW	BW pole[a]	Mod		|133|	|58|	|75|	Mod

D15 Saclay (EPSA) Only

	Origin \ Parameter		Mass	$\Gamma_{(total)}$	$\Gamma_{(N\pi)}$	$\Gamma_{[\Delta\pi(D)]}$	
K-matrix	K-matrix pole	Real	1682	154	64	90	Real
K-matrix	T-matrix	Real	1660	122	53	69	Real
K-matrix		Imag	$\frac{-138i}{2}$	-44i	-20i	-24i	Imag
K-matrix	pole[a]	Mod		|129|	|56|	|73|	Mod
UB+BW	UB+BW BW parameter	Real	1684	150	62	88	Real
UB+BW	UB+BW	Real	1663		56		Real
UB+BW		Imag	$\frac{-143i}{2}$		-15i		Imag
UB+BW	BW pole[a]	Mod			58		Mod

[a] T-matrix pole has complex position and partial width (Γ_i). Modulus of $\Gamma_{(total)}$ is the sum of the moduli of Γ_i.

Table V c

3 Channel, Large Background, F35 CERN(EPSA)+Nππ

	Origin \ Parameter		Mass	$\Gamma_{(total)}$	$\Gamma_{(N\pi)}$	$\Gamma_{[\Delta\pi(F)]}$	$\Gamma_{[N\rho_{3/2}(P)]}$	
K-matrix	K-matrix pole from Table III	Real	2169	3401	178	47^{+}	3177^{-}	Real
K-matrix	T-matrix pole[a] from Table IV	Real	1824	35	36	19^{+}	-20^{-}	Real
K-matrix		Imag	$\frac{-282i}{2}$	-148i	-26i	-17i	-105i	Imag
K-matrix		Mod		|177|	|44|	|26|	|107|	Mod
U(UB+BW)	Unitarized (UB+BW) BW parameter	Real	1907	325	51	55^{+}	219^{-}	Real
U(UB+BW)	Unitarized (UB+BW) BW pole[a]	Real	1824	53	43	16^{+}	-6^{-}	Real
U(UB+BW)		Imag	$\frac{-282i}{2}$	-143i	-27i	-12i	-99i	Imag
U(UB+BW)		Mod		|173|	|51|	|23|	|99|	Mod
UB+BW	UB+BW BW parameter	Real	1957	391	75	41^{+}	275^{-}	Real
UB+BW	UB+BW BW pole[a]	Real	1783	13	37	18^{+}	-42^{-}	Real
UB+BW		Imag	$\frac{-386i}{2}$	-304i	-62i	-36i	-206i	Imag
UB+BW		Mod		|323|	|72|	|41|	|210|	Mod

F35 CERN (EPSA) Only

	Origin \ Parameter		Mass	$\Gamma_{(total)}$	$\Gamma_{[\Delta\pi(F)]}$		
K-matrix	K-matrix pole	Real	2042	1746	154	1592	Real
K-matrix	T-matrix pole[a]	Real	1810		33		Real
K-matrix		Imag	$\frac{-275i}{2}$		-25i		Imag
K-matrix		Mod			|42|		Mod
UB+BW	UB+BW BW parameter	Real	1891	300	36	264	Real
UB+BW	UB+BW BW pole[a]	Real	1815		20		Real
UB+BW		Imag	$\frac{-222i}{2}$		-13i		Imag
UB+BW		Mod			|24|		Mod

[a] T-matrix pole has complex position and partial width (Γ_i). Modulus of $\Gamma_{(total)}$ is the sum of the moduli of Γ_i.

Table V d

3 Channel, Large Background, F35 Saclay (EPSA)+Nππ

Origin \ Parameter		Mass	$\Gamma_{(total)}$	$\Gamma_{(N\pi)}$	$\Gamma_{[\Delta\pi(F)]}$	$\Gamma_{[N\rho_{3/2}(P)]}$	
K-matrix pole from Table III	Real	2136	2545	165	135^{+}	2246^{-}	Real
T-matrix pole[a] from Table IV	Real	1832	35	36	16^{+}	-17^{-}	Real
	Imag	$\frac{-278i}{2}$	-152i	-25i	-19i	-108i	Imag
	Mod		|178|	44	25	|109|	Mod
Unitarized (UB+BW) BW parameter	Real	1911	320	50	50^{+}	220^{-}	Real
Unitarized (UB+BW) BW pole[a]	Real	1833	50	46	15^{+}	-11^{-}	Real
	Imag	$\frac{-282i}{2}$	-146i	-25i	-14i	-106i	Imag
	Mod		|180|	53	21	106	Mod
UB+BW BW parameter	Real	1942	395	70	47^{+}	278^{-}	Real
UB+BW BW pole[a]	Real	1798	-10	39	15^{+}	-64^{-}	Real
	Imag	$\frac{-363i}{2}$	-290i	-52i	-36i	-202i	Imag
	Mod		|316|	|65|	|39|	212	Mod

F35 Saclay (EPSA) Only

Origin \ Parameter		Mass	$\Gamma_{(total)}$	$\Gamma_{(N\pi)}$	$\Gamma_{[\Delta\pi(F)]}$	
K-matrix pole	Real	2062	1808	156	1652	Real
T-matrix pole[a]	Real	1822		35		Real
	Imag	$\frac{-283i}{2}$		-26i		Imag
	Mod			|43|		Mod
UB+BW BW parameter	Real	1901	291	35	256	Real
UB+BW BW pole[a]	Real	1833		22		Real
	Imag	$\frac{-219i}{2}$		-11i		Imag
	Mod			24		Mod

[a] T-matrix pole has complex position and partial width (Γ_i). Modulus of $\Gamma_{(total)}$ is the sum of the moduli of Γ_i.

Table V e

4 Channel, Medium Background, F15 CERN+Nππ

Origin \ Parameter		Mass	$\Gamma_{(total)}$	$\Gamma_{(N\pi)}$	$\Gamma_{[\Delta\pi(P)]}$	$\Gamma_{[N\rho_{3/2}(P)}$	$\Gamma_{[N\epsilon(D)]}$	
K-matrix pole from Table III	Real	1684	156	83	5 $^{+}$	53 $^{+}$	15 $^{+}$	Real
T-matrix pole [a] from Table IV	Real	1672	152	99	5 $^{+}$	33 $^{+}$	15 $^{+}$	Real
	Imag	$\frac{-155i}{2}$	-49i	-17i	11i	-27i	-16i	Imag
	Mod		|176|	|101|	|12|	|42|	|21|	Mod
Unitarized (UB+BW) BW parameter	Real	1681	149	86	16 $^{+}$	31 $^{+}$	16 $^{+}$	Real
Unitarized BW pole [a]	Real	1672	148	92	7 $^{+}$	37 $^{+}$	12 $^{+}$	Real
		$\frac{-148i}{2}$	-33i	-11i	8i	-14i	-14i	Imag
	Mod		|162|	|92|	|11|	|40|	|19|	Mod
UB+BW BW parameter	Real	1679	148	84	12 $^{+}$	36 $^{+}$	16 $^{+}$	Real
UB+BW BW pole [a]	Real	1672	152	93	10 $^{+}$	37 $^{+}$	13 $^{+}$	Real
	Imag	$\frac{-147i}{2}$	-30i	-10i	-9i	-18i	-11i	Imag
	Mod		|165|	|93|	|14|	|41|	|17|	Mod

F15 CERN (EPSA) Only

Origin \ Parameter		Mass	$\Gamma_{(total)}$	$\Gamma_{(N\pi)}$	$\Gamma_{[\Delta\pi(P)]}$	
K-matrix pole	Real	1693	183	107	77	Real
T-matrix pole [a]	Real	1659		70		Real
	Imag	$\frac{-128i}{2}$		-24i		Imag
	Mod			|74|		Mod
UB+BW BW parameter	Real	1678	135	82	53	Real
UB+BW BW pole [a]	Real	1664		75		Real
	Imag	$\frac{-129i}{2}$		-15i		Imag
	Mod			|77|		Mod

[a] T-matrix pole has complex position and partial width (Γ_i). Modulus of $\Gamma_{(total)}$ is the sum of the moduli of Γ_i.

Table V f

4 Channel, Medium Background, F15 Saclay (EPSA)+$N\pi\pi$

	Origin \ Parameter		Mass	$\Gamma_{(total)}$	$\Gamma_{(N\pi)}$	$\Gamma_{[\Delta\pi(p)]}$	$\Gamma_{[N\rho_{3/2}(p)]}$	$\Gamma_{[N\epsilon(D)]}$	
K-matrix	K-matrix pole from Table III	Real	1682	152	81	7^+	50^+	14^+	Real
K-matrix	T-matrix pole [a] from Table IV	Real	1669	138	89	7^+	30^+	12^+	Real
		Imag	$\frac{-145i}{2}$	-51i	-20i	9i	-25i	-15i	Imag
		Mod		| 161 |	| 91 |	| 12 |	| 39 |	| 19 |	Mod
U(UB+BW)	Unitarized (UB+BW) BW parameter	Real	1678	142	81	16^+	30^+	15^+	Real
U(UB+BW)	Unitarized (UB+BW) BW pole [a]	Real	1669	137	84	8^+	35^+	10^+	Real
		Imag	$\frac{-140i}{2}$	-35i	-12i	7i	-15i	-15i	Imag
		Mod		| 151 |	| 85 |	| 11 |	| 38 |	| 17 |	Mod
UB+BW	UB+BW BW parameter	Real	1679	141	80	12^+	34^+	15^+	Real
UB+BW	UB+BW BW pole [a]	Real	1672	144	87	10^+	35^+	12^+	Real
		Imag	$\frac{-140i}{2}$	-25i	-7i	9i	-16i	-11i	Imag
		Mod		| 154 |	| 87 |	| 13 |	| 38 |	| 16 |	Mod

F15 Saclay (EPSA) Only

	Origin \ Parameter		Mass	$\Gamma_{(total)}$	$\Gamma_{(N\pi)}$	$\Gamma_{[\Delta\pi(P)]}$	
K-matrix	K-matrix pole	Real	1692	179	104	75	Real
K-matrix	T-matrix pole [a]	Real	1658		64		Real
		Imag	$\frac{-121i}{2}$		-26i		Imag
		Mod			| 69 |		Mod
UB+BW	UB+BW BW parameter	Real	1677	77	50		Real
UB+BW	UB+BW BW pole [a]	Real	1665		71		Real
		Imag	$\frac{-122i}{2}$		-13i		Imag
		Mod			| 73 |		Mod

[a] T-matrix pole has complex position and partial width (Γ_i). Modulus of $\Gamma_{(total)}$ is the sum of the moduli of Γ_i.

Table VI. Sign of all couplings from Breit-Wigner refit made by eyeball in sequence S, P, D. F.

Table VIa

Wave	S11 CERN, First pole			
Channel	N π, L = 0	N ϵ, L = 1	N $\rho_{1/2}$, L = 0	N η[a], L = 0
Sign coupling	+	+	+	+
Angle	-20°	10°	-10°	40°

Wave	S11 Saclay, First pole			
Channel	N π, L = 0	N ϵ, L = 1	N $\rho_{1/2}$, L = 0	N η[a], L = 0
Sign coupling	+	+	+	+
Angle	-20°	20°	-20°	40°

Wave	S11 CERN, Second pole			
Channel	N π, L = 0	N ϵ, L = 1	N $\rho_{1/2}$, L = 0	N η, L = 0
Sign coupling	+	-	+	-
Angle	-20°	-40°	-40°	-30°

[a] N η channel is not in N $\pi\pi$; this sign has been defined as positive.

Table VIb

Wave	S11 Saclay, Second Pole			
Channel	N π, L = 0	N ϵ, L = 1	N $\rho_{1/2}$, L = 0	N η, L = 0
Sign coupling	+	-	+	-
Angle	20°	-40°	-40°	-20°

	S31 CERN		
Channel	N π, L = 0	Δ π, L = 2	N $\rho_{1/2}$, L = 0
Sign coupling	+	-	-
Angle	-45°	0°	45°

	S31 Saclay		
Channel	N π, L = 0	Δ π, L = 2	N $\rho_{1/2}$, L = 0
Sign coupling	+	-	-
Angle	-45°	0°	45°

Table VIc

Wave	P11 CERN, First Pole		
Channel	N π, L = 1	Δ π, L = 1	N ϵ, L = 0
Sign coupling	+	+	-
Angle	-30°	-60°	-40°

Wave	P11 Saclay, First Pole		
Channel	N π, L = 1	Δ π, L = 1	N ϵ, L = 0
Sign coupling	+	+	-
Angle	-30°	-60°	-40°

Wave	P11 CERN, Second Pole		
Channel	N π, L = 1	Δ π, L = 1	N ϵ, L = 0
Sign coupling	+	-	+
Angle	-50°	-10°	-40°

Table VId

Wave	P11 Saclay, Second Pole		
Channel	N π, L = 1	$\Delta\pi$, L = 1	N ϵ, L = 0
Sign coupling	+	-	+
Angle	-50°	-10°	-30°

Wave	P13 CERN	
Channel	N π, L = 1	N $\rho_{1/2}$, L = 1
Sign coupling	+	-
Angle	-45°	-45°

Wave	P13 Saclay	
Channel	N π, L = 1	N $\rho_{1/2}$, L = 1
Sign coupling	+	-
Angle	-45°	-45°

Table VIe

Wave	D13 CERN, First Pole				
Channel	N π, L = 2	Δ π, L = 0	N $\rho_{3/2}$, L = 0	N ϵ, L = 1	Δ π, L = 2
Sign coupling	+	-	+	+	-
Angle	5°	35°	5°	-65°	-5°

Wave	D13 Saclay, First Pole				
Channel	N π, L = 2	Δ π, L = 0	N $\rho_{3/2}$, L = 0	N ϵ, L = 1	Δ π, L = 2
Sign coupling	+	-	+	+	-
Angle	5°	35°	5°	-65°	-5°

Wave	D13 CERN, Second Pole				
Channel	N π, L = 2	Δ π, L = 0	N $\rho_{3/2}$, L = 0	N ϵ, L = 1	Δ π, L = 2
Sign coupling	+	+	-	-	-
Angle	-20°	-60°	70°	-80°	-60°

Table VIf

Wave	D13 Saclay, Second Pole				
Channel	N π, L = 2	Δ π, L = 0	N $\rho_{3/2}$, L = 0	N ϵ, L = 1	Δ π, L 2
Sign coupling	+	+	-	-	-
Angle	-20°	-60°	70°	-80°	-60°

Wave	D13 CERN, Third Pole				
Channel	N π, L = 2	Δ π, L = 0	N $\rho_{3/2}$, L = 0	N ϵ, L = 1	Δ π, L = 2
Sign coupling	+	+	-	?	?
Angle	-40°	80°	-40°	?	?

Wave	D13 Saclay, Third Pole				
Channel	N π, L = 2	Δ π, L = 0	N $\rho_{3/2}$, L = 0	N ϵ, L = 2	Δ π, L 2
Sign coupling	+	+	-	?	?
Angle	-40°	80°	-40°	?	?

Table VI g

Wave	D33 CERN		
Channel	$N\pi$, L = 2	$\Delta\pi$, L = 0	$N\rho_{3/2}$, L = 0
Sign coupling	+	+	+
Angle	-30°	-60°	0°

Wave	D33 Saclay		
Channel	$N\pi$, L = 2	$\Delta\pi$, L = 0	$N\rho_{3/2}$, L = 0
Sign coupling	+	+	+
Angle	-30°	-60°	0°

Wave	D15 CERN	
Channel	$N\pi$, L = 2	$\Delta\pi$, L = 2
Sign coupling	+	-
Angle	-10°	-20°

Table VIh

Wave	D15 Saclay			
Channel	N π, L = 2	Δ π, L = 2		
Sign coupling	+	-		
Angle	-10°	-20°		

Wave	F15 CERN			
Channel	N π, L = 3	Δ π, L = 1	N $\rho_{3/2}$, L = 1	N ε, L = 2
Sign coupling	+	+	+	-
Angle	-10°	10°	-10°	-30°

Wave	F15 Saclay			
Channel	N π, L = 3	Δ π, L = 1	N $\rho_{3/2}$, L = 1	N ε, L = 2
Sign coupling	+	+	+	+
Angle	-10°	10°	-10°	-30°

Table VI i

Wave	F35 CERN		
Channel	$N\pi$, L = 3	$\Delta\pi$, L = 3	$N\rho_{3/2}$, L = 1
Sign coupling	+	+	-
Angle	-25°	-50°	-75°

Wave	F 35 Saclay		
Channel	$N\pi$, L 3	$\Delta\pi$, L 3	$N\rho_{3/2}$, L = 1
Sign coupling	+	+	-
Angle	-25°	-50°	-75°

Wave	F 37 CERN			
Channel	$N\pi$, L = 3	$\Delta\pi$, L = 3	$N\rho_{3/2}$, L = 3	$\Delta\rho$, L 1
Sign coupling	+	+	-	+[a]
Angle	-10°	20°	-80°	-40°

[a] $\Delta\rho$ channel is not in $N\pi\pi$; its sign has been defined as positive.

Table VIj

Channel	$N\pi$, L = 3	$\Delta\pi$, L = 3	$N\rho_{3/2}$, L = 3	$\Delta\rho$, L = 1
Sign coupling	+	+	-	+ [a]
Angle	-10°	20°	-80°	-40°

[a] $\Delta\rho$ channel is not in $N\pi\pi$; its sign has been defined as positive.

Table VII. Cross-section ratio for ηN, assuming S-wave dominance at 1520-1590 MeV, c.m.

Energy	1520	1530	1540	1560	1590
C_0	.120	.125	.125	.130	.10
C_1	.025	.025	.025	.01	0.0
$\frac{\sigma_{P11}}{\sigma_{S11}}$	.01	.01	.01	.0015	0.0
C_2	.01	.045	.055	.07	.06
$\frac{\sigma_{D13}}{\sigma_{S11}}$(only)	.001	.016	.024	.036	.045
$\frac{\sigma_{D15}}{\sigma_{S11}}$(only)	.001	.010	.016	.024	.03
C_3	0.0	0.0	0.0	0.0	-.05
$\frac{\sigma_{F15}}{\sigma_{S11}}$	0.0	0.0	0.0	0.0	.02

FIGURE CAPTIONS

Fig. 1. S-channel diagram for isobar α outgoing and isobar β incoming, where $B(q, \ell)$ is square root of Blatt-Weisskopf[8] barrier factor for momentum q in an angular momentum state ℓ. W_α is the Watson final state factor for the α isobar. A_α is the elastic Argand amplitude for particles that make up the isobar.

Fig. 2. Diagram of $1-\eta^2$ for the six different resonances used in determining the overall phase.

Fig. 3. Flow diagram for the reduction of four sets of ϕ_i's to one set of ϕ_i's, using Eqs. (33) and (35).

Fig. 4.1. Argand diagrams and partial wave cross sections for the elastic and inelastic channels. The smooth curve on the Argand diagrams is the amplitude obtained from the K-matrix when the description was possible. Cross-hatched marks on the curve correspond to the energies D, E, F, etc. the arrows indicate the known resonances of Table V. The total inelastic contribution in each elastic wave (ϕ) is compared with the sum of the inelastic contributions we observe ($\divideontimes$). Facing each inelastic Argand diagram, we give the variation with energy of the square modulus of the wave. (This caption also applies to Figs. 4.2 through 4.16.)

Fig. 5. Three different paths $\Delta, \Delta', \Delta''$ in the E plane. E is the diparticle mass that makes up the isobar. W is the complex $\sqrt{s}$ (three body) where one searches for poles in the three-body T-matrix.

Fig. 6. The paths of Fig. 5 deformed so that they only differ by integration around the pole.

Fig. 7. The branch cuts in the $\sqrt{s}$ or W plane (total c.m. energy) generated by the pole in the final state interaction of the isobar.

Fig. 8. Three different paths of integration in the E plane at four different values of W. The dashed line is the projection of the branch cut from the W plane which is not crossed by $W-m_3$ as it moves from (a) to (d).

Fig. 9. Three points on the Δ, Δ', and Δ'' sheets and how one has to travel from them to the physical region in a continuous way.

Fig. 10. The poles of the F15 T-matrix which lies near ρN threshold. Each sheet is generated by the ρN cut.

Fig. 11. Argand diagrams from U(UB + BW) refit to F35 wave. Solid line is the U(UB + BW) amplitude, while dashed line is the unitary background UB. Energy range is from 1740 to 1900 MeV, where arrows point direction of increasing energy. $\Delta\theta_i$ is the change of rotation angle of Breit-Wigner in this energy range. See Eq. (65).

Fig. 12. K-matrix prediction for $N\eta$ S11 first moment plotted against total cross section.

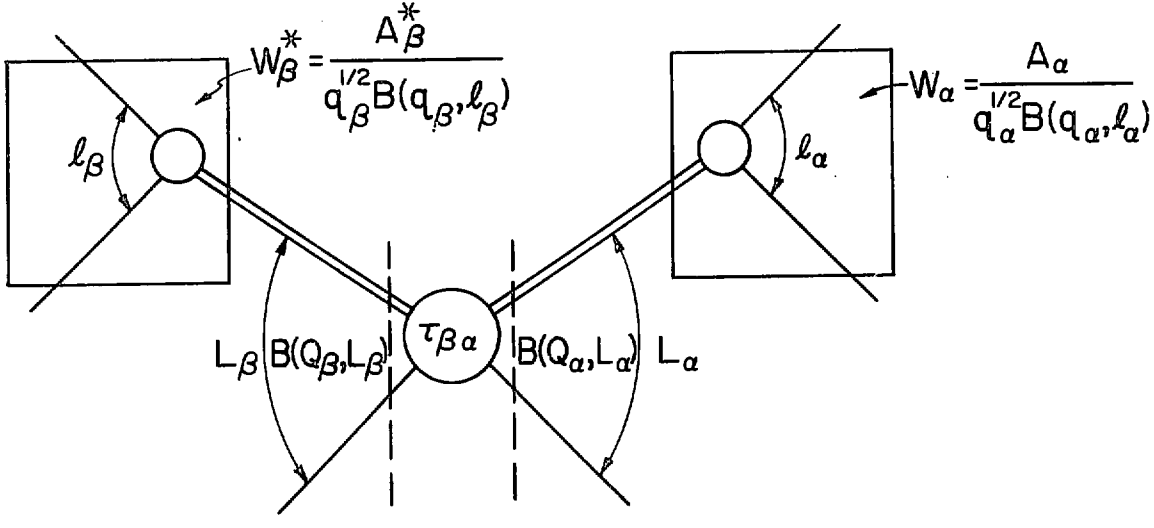

XBL7311-4466

Fig. 1.

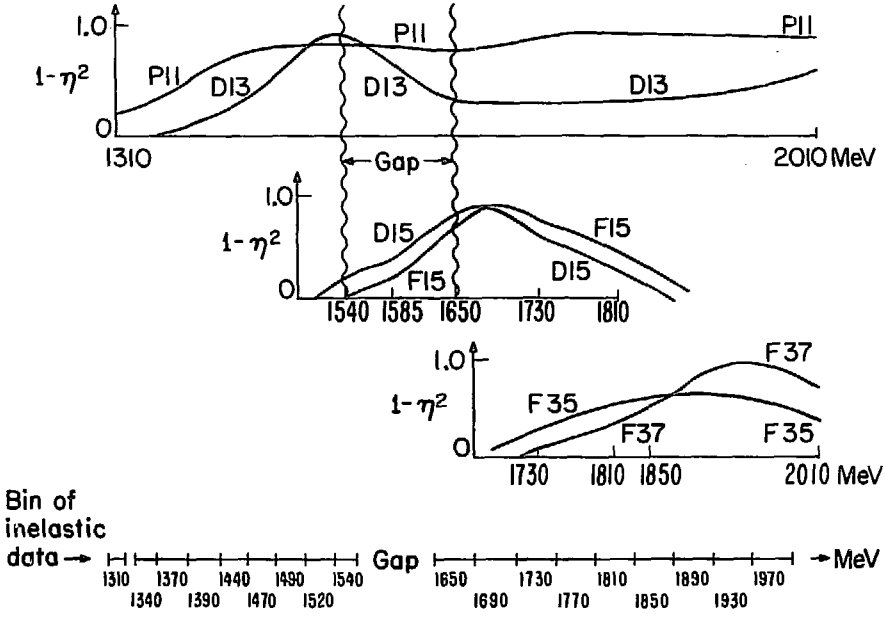

XBL7311-4464

Fig. 2.

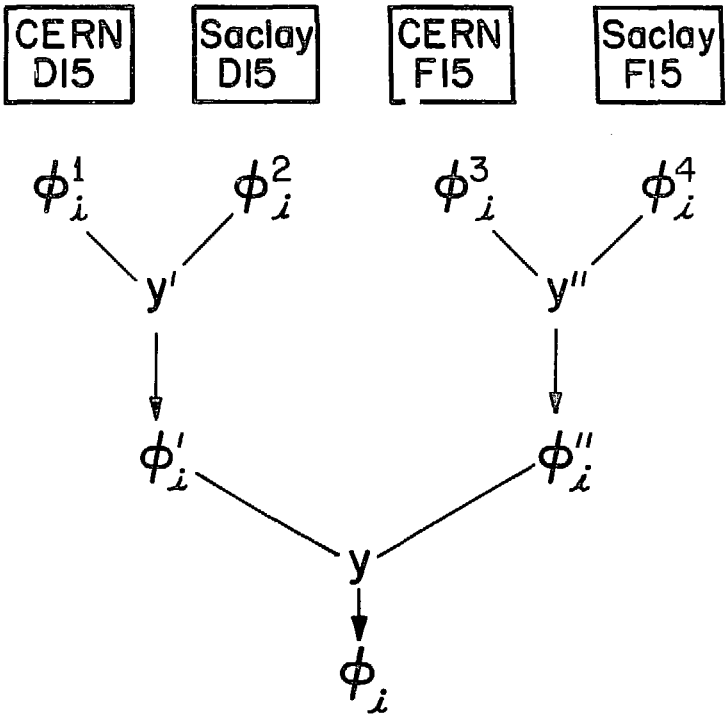

XBL7311-4465

Fig. 3.

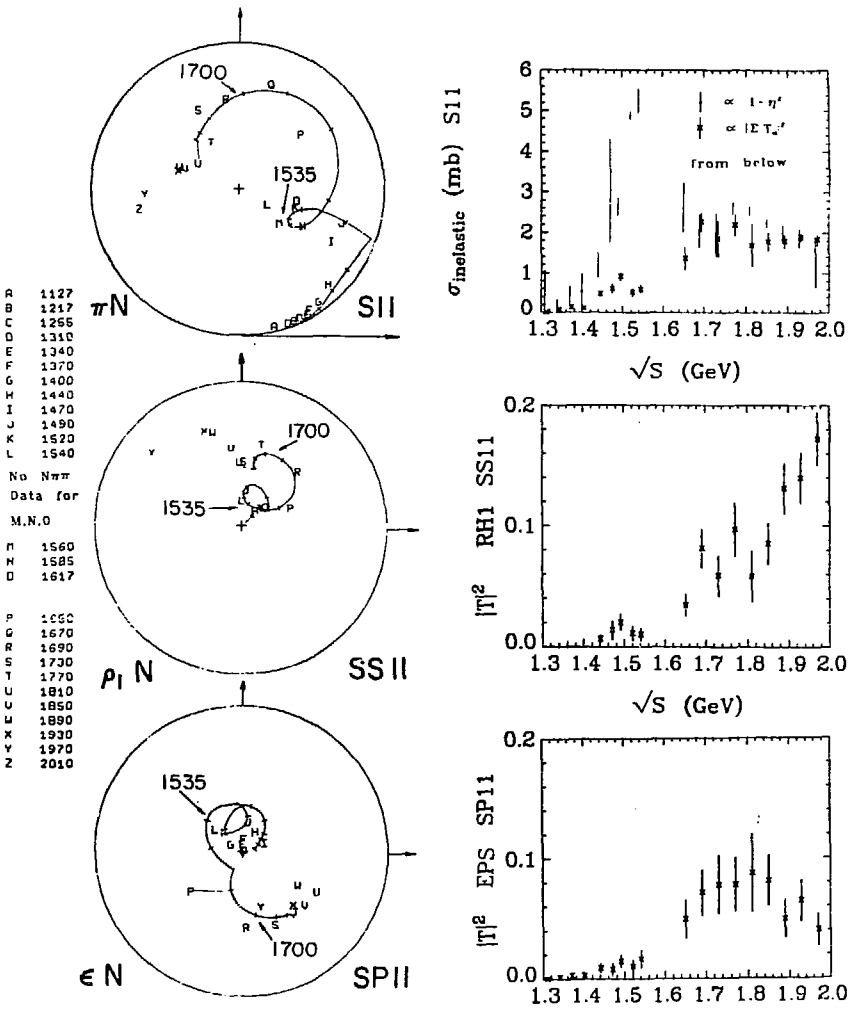

Figure 4.1

XBL 728-1512

$I = \frac{1}{2}$ πN S11

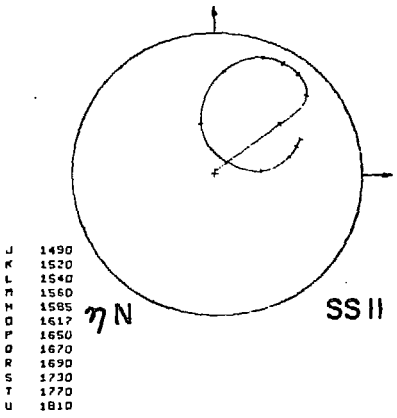

ETA - N SS11

NO DATA USED IN FIT

Figure 4.2

XBL 738-1041

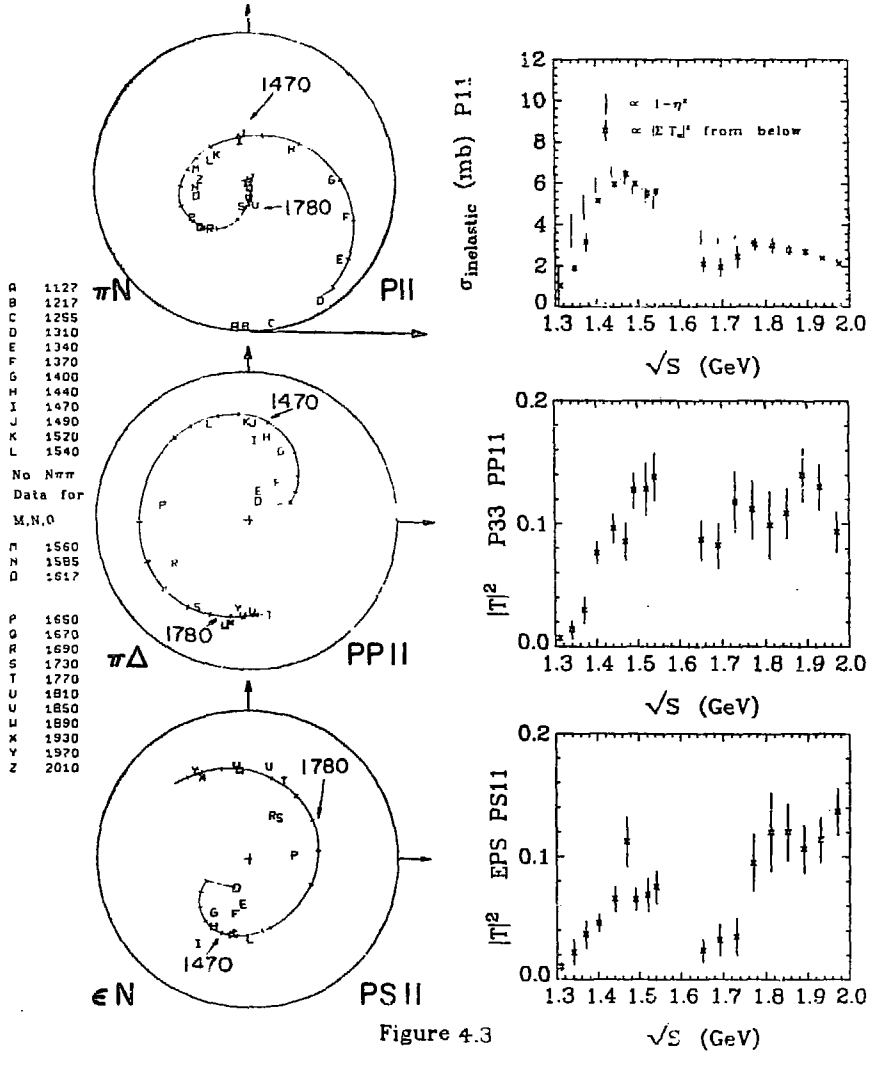

Figure 4.3

XBL 728-1513

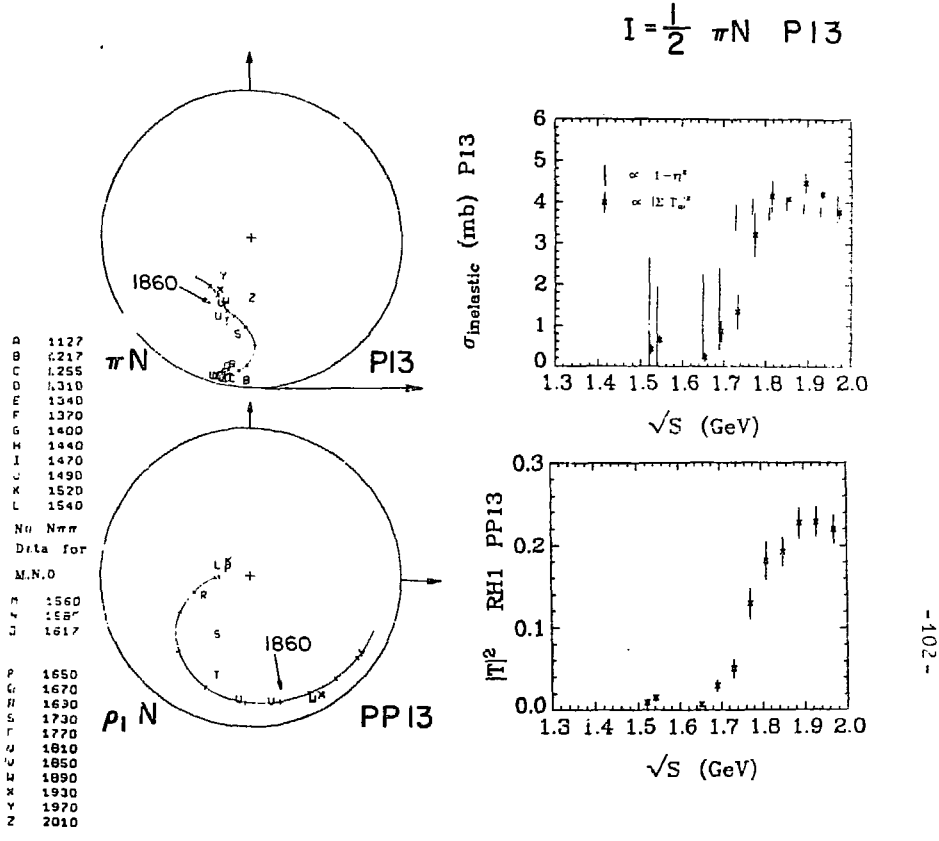

Figure 4.4

XBL 728-1514

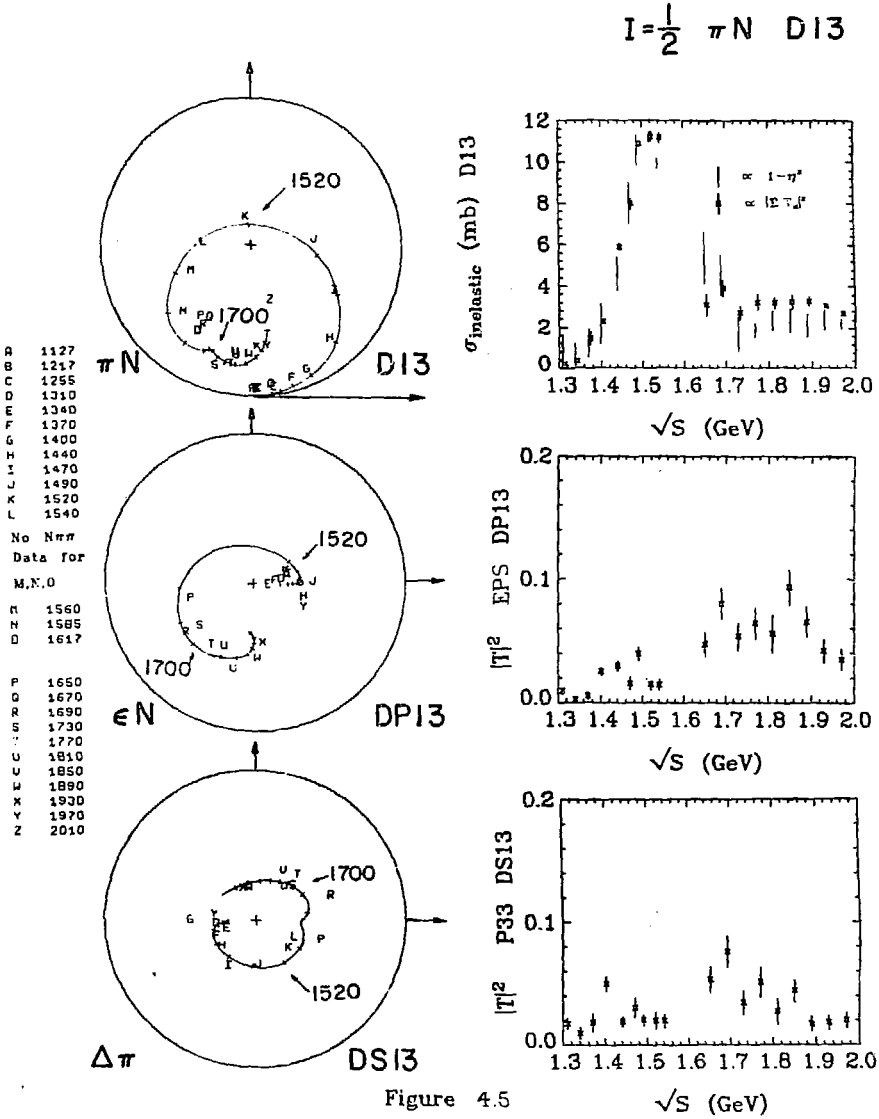

Figure 4.5

XBL 728-1515

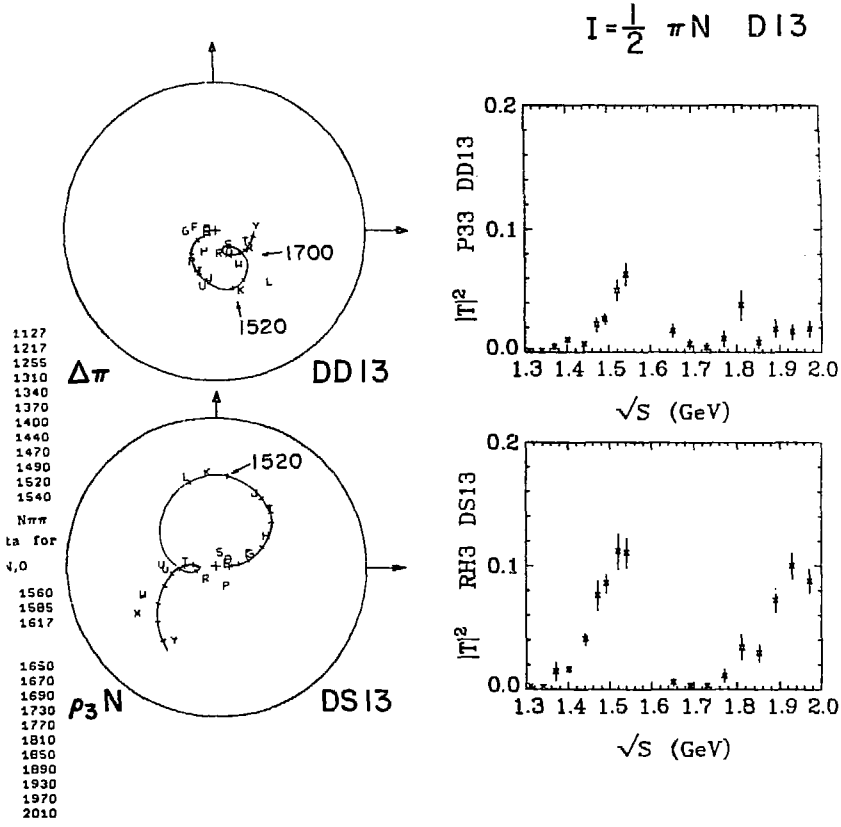

Figure 4.6

XBL 728-1516

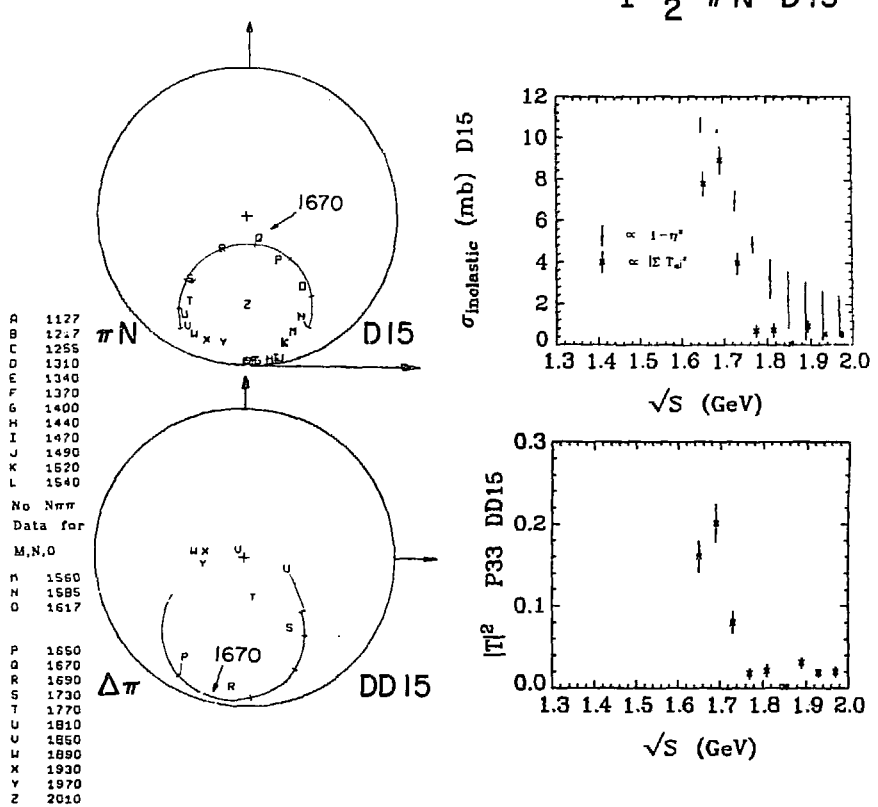

Figure 4.7

XBL 728-1517

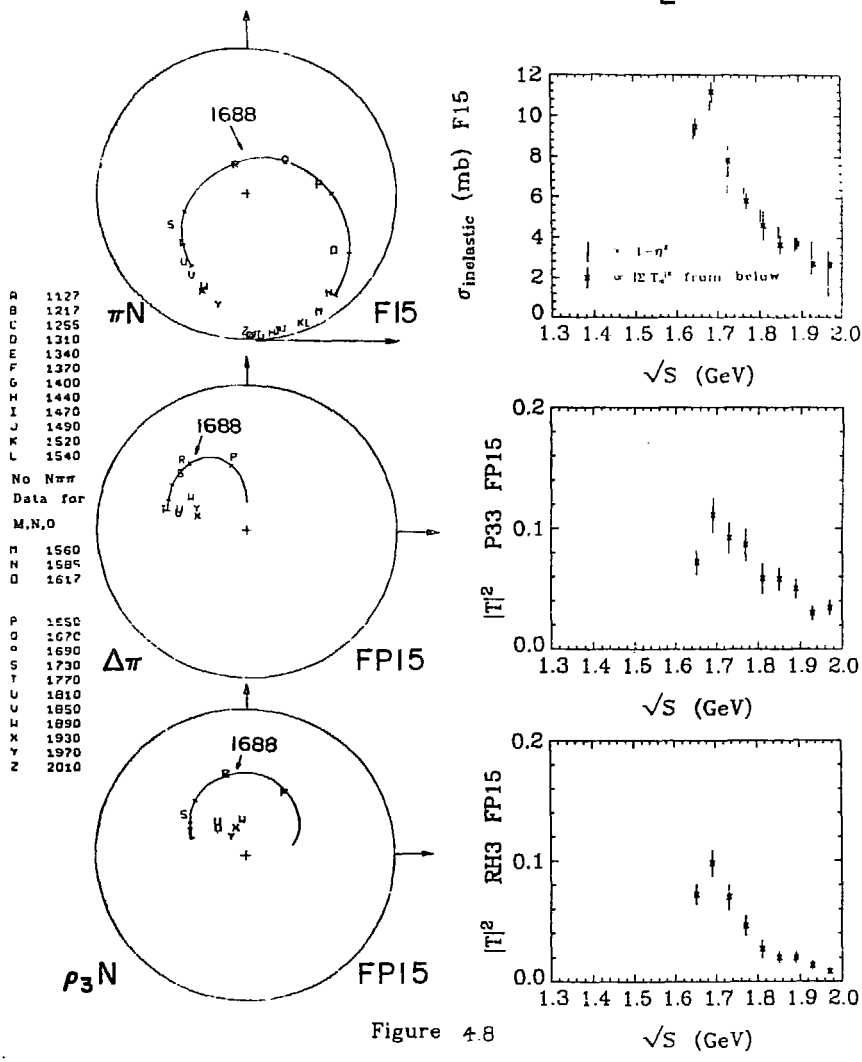

Figure 4.8

XBL 728-1518

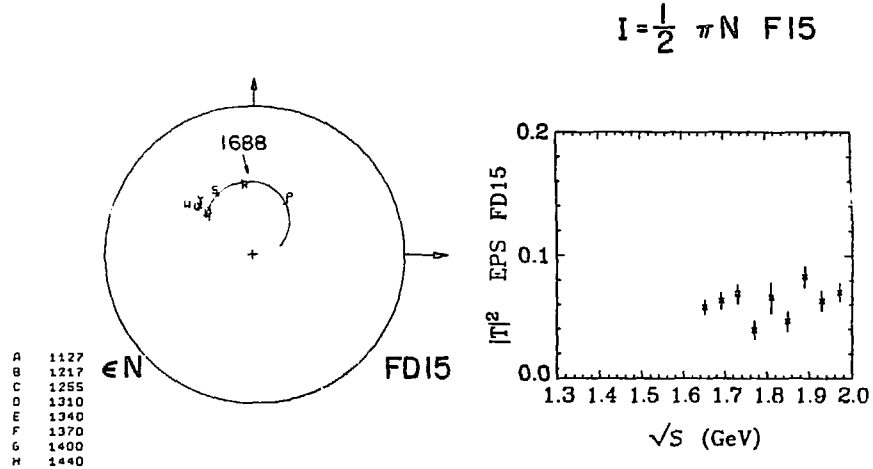

A	1127
B	1217
C	1255
D	1310
E	1340
F	1370
G	1400
H	1440
I	1470
J	1490
K	1520
L	1540

No Nππ

Data for

M,N,O

M	1560
N	1595
O	1617

P	1650
Q	1670
R	1690
S	1730
T	1770
U	1810
V	1850
W	1890
X	1930
Y	1970
Z	2010

Figure 4.9

XBL 728-1519

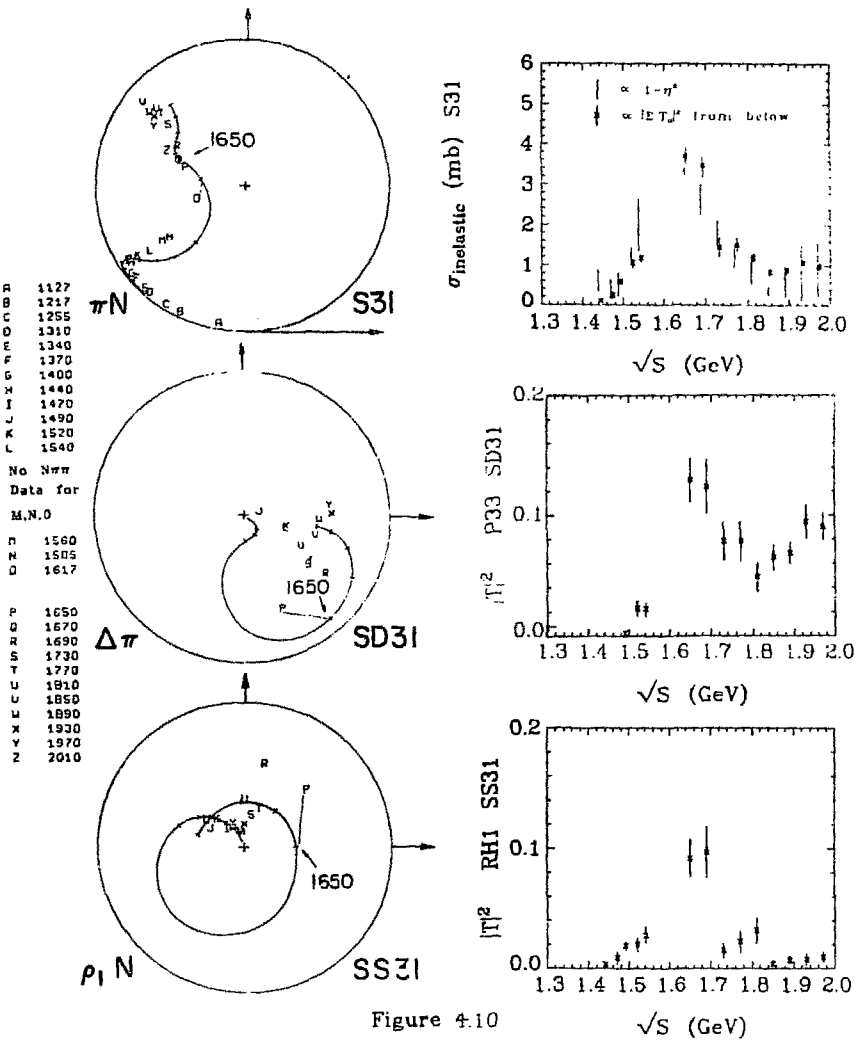

Figure 4.10

XBL 728-1520

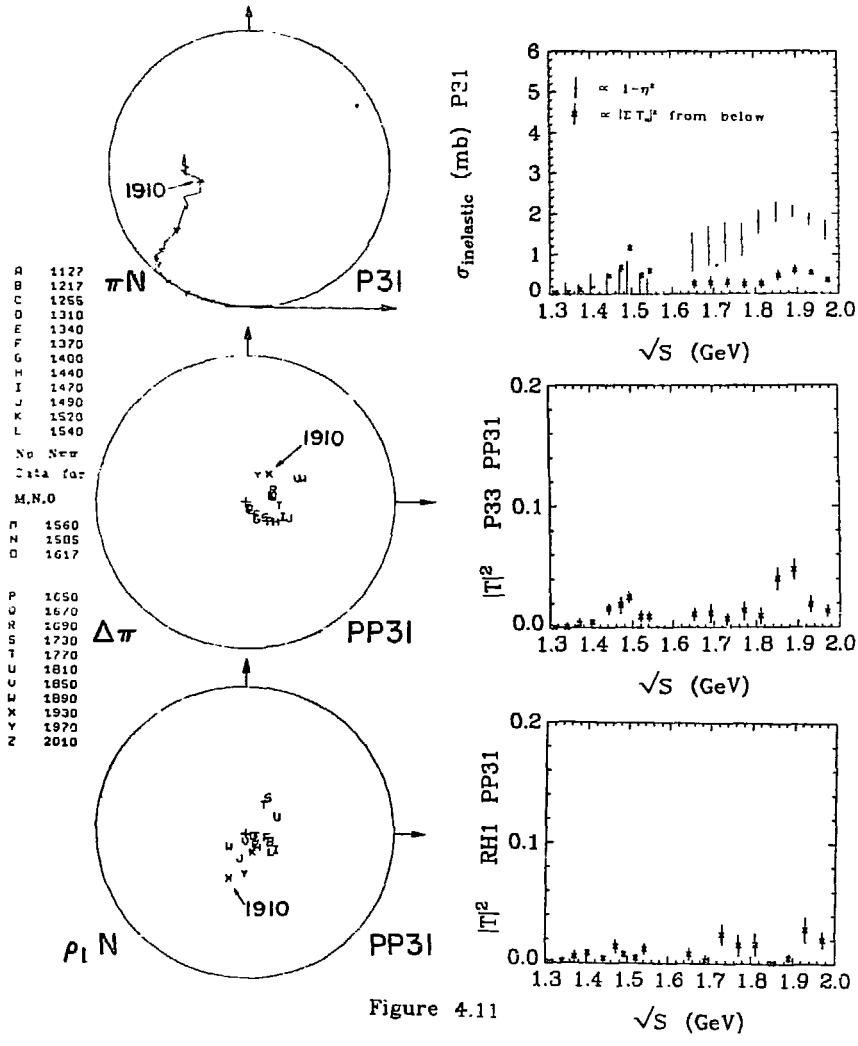

Figure 4.11

XBL 728-1521

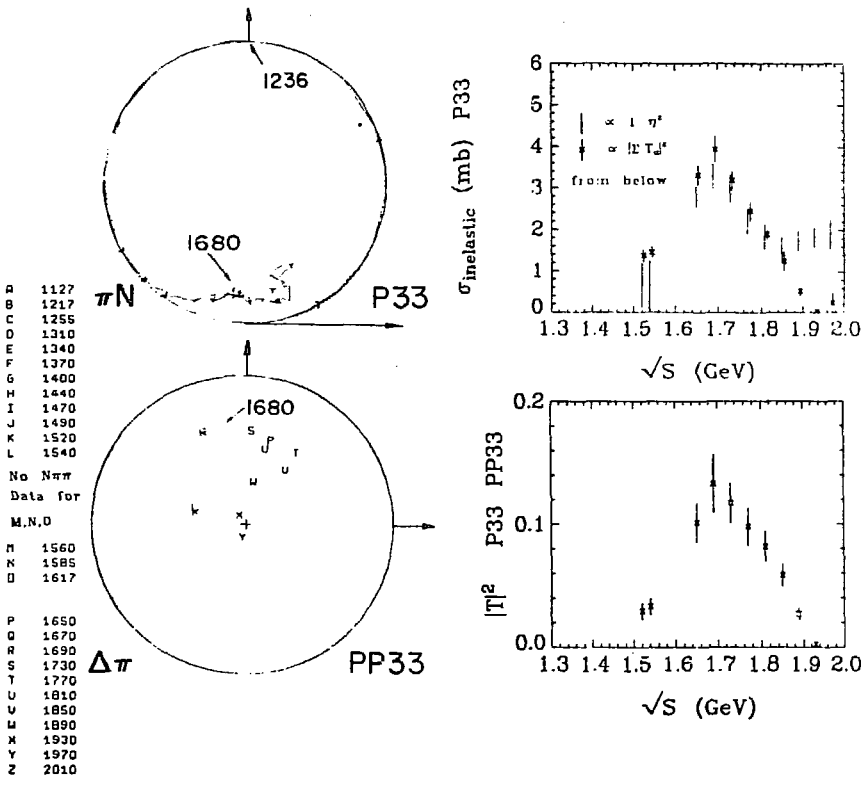

Figure 4.12

XBL 728-1522

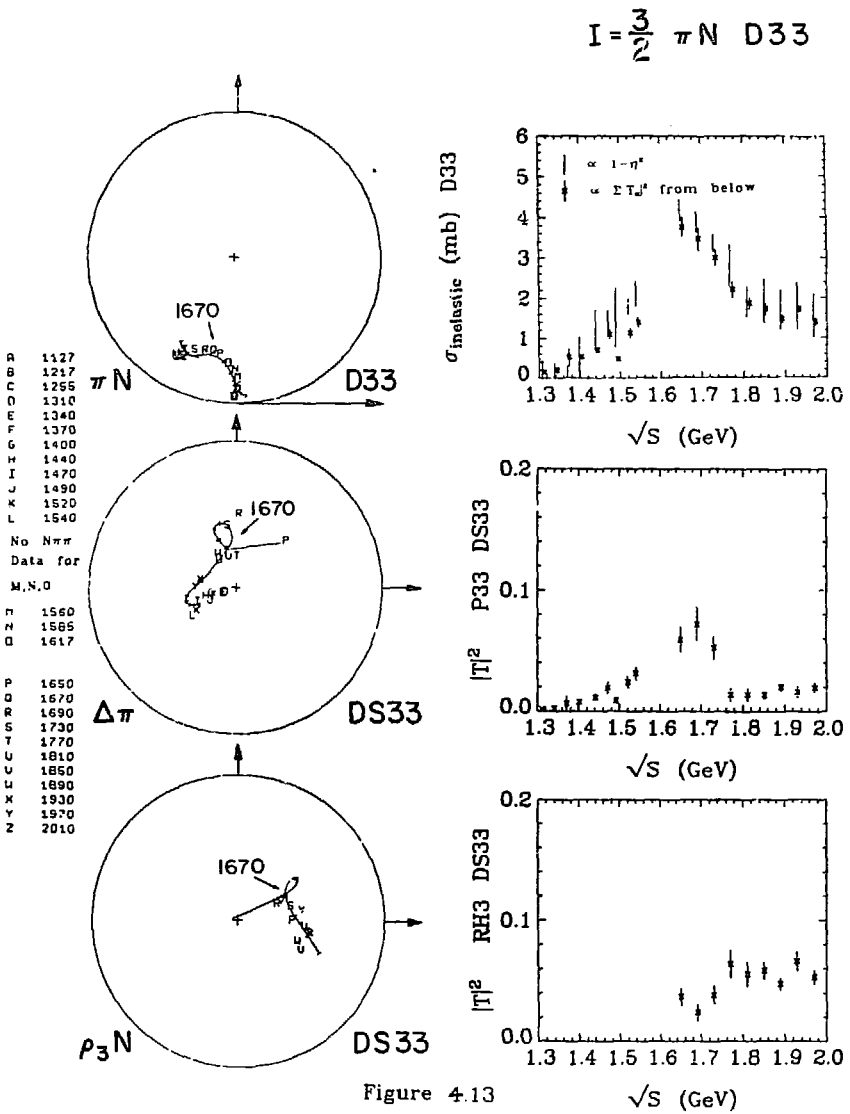

Figure 4.13

XBL 728-1523

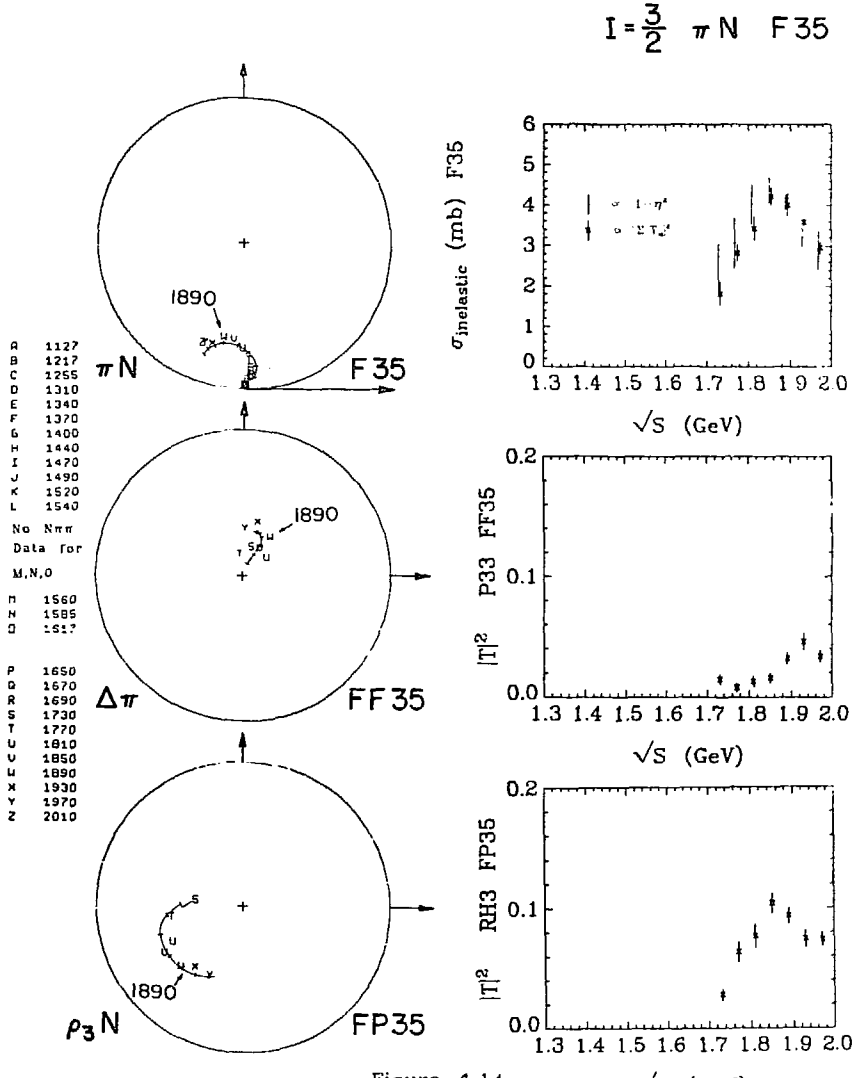

Figure 4.14

XBL 728-1524

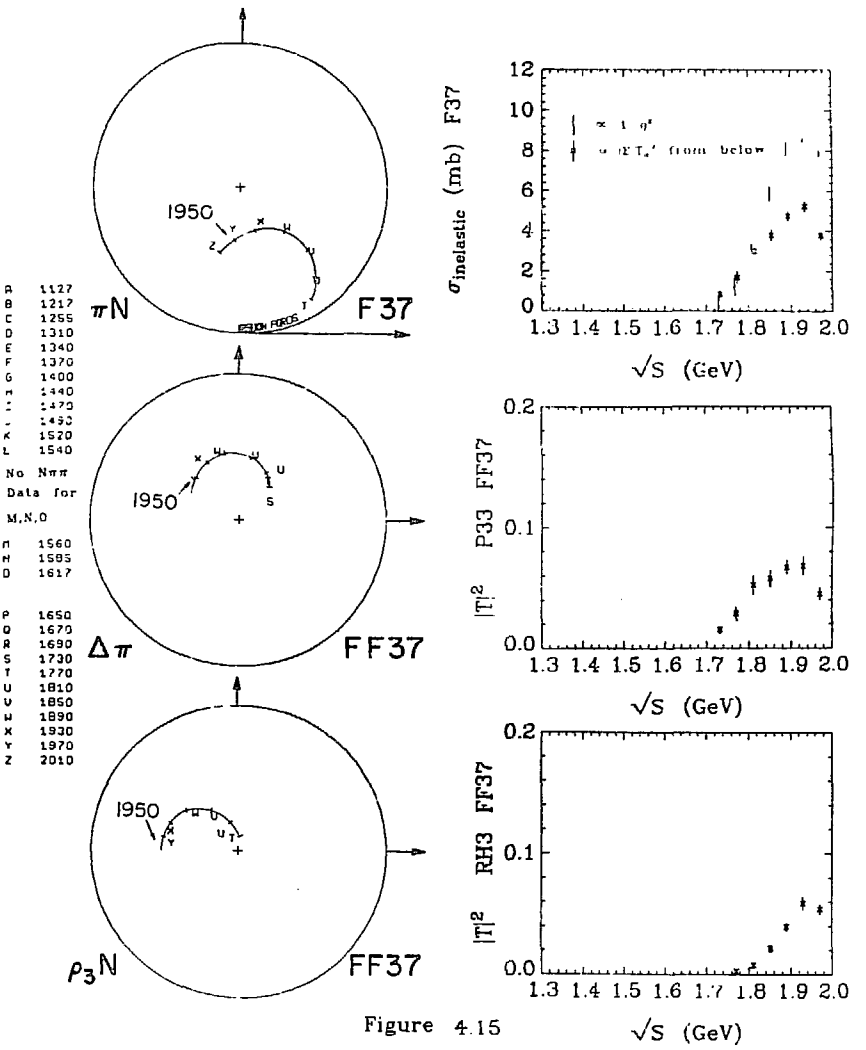

Figure 4.15

XBL 728-1525

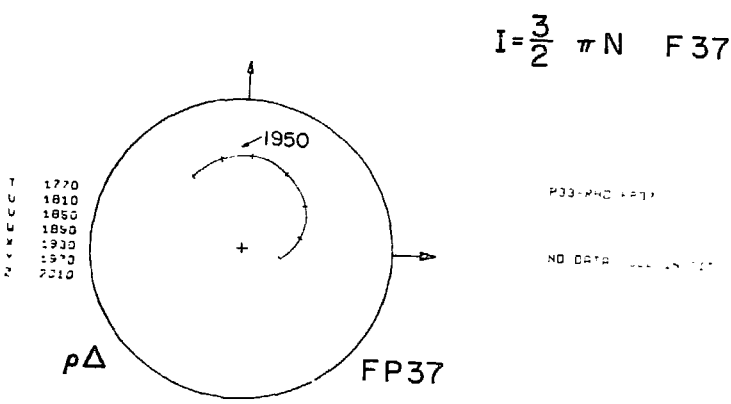

Figure 4.16

XBL 728-1526

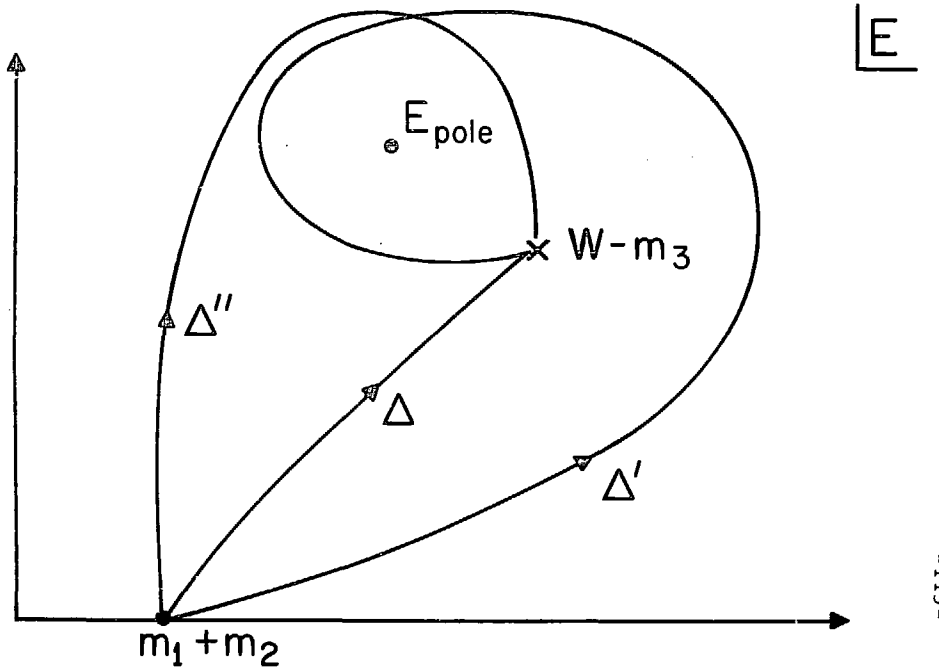

XBL7311-4467

Fig. 5.

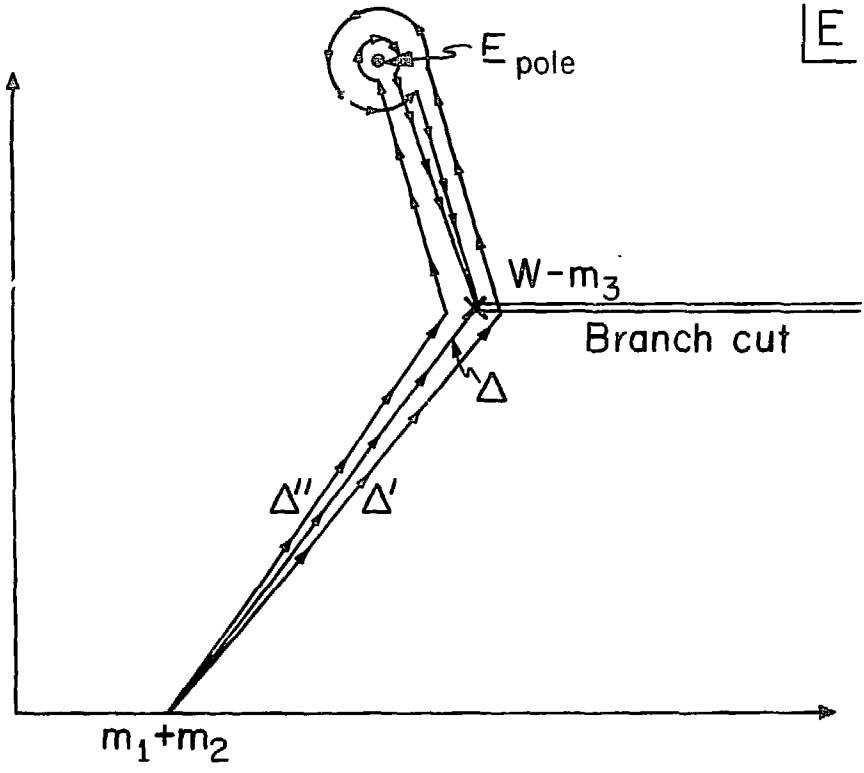

XBL7311-4468

Fig. 6.

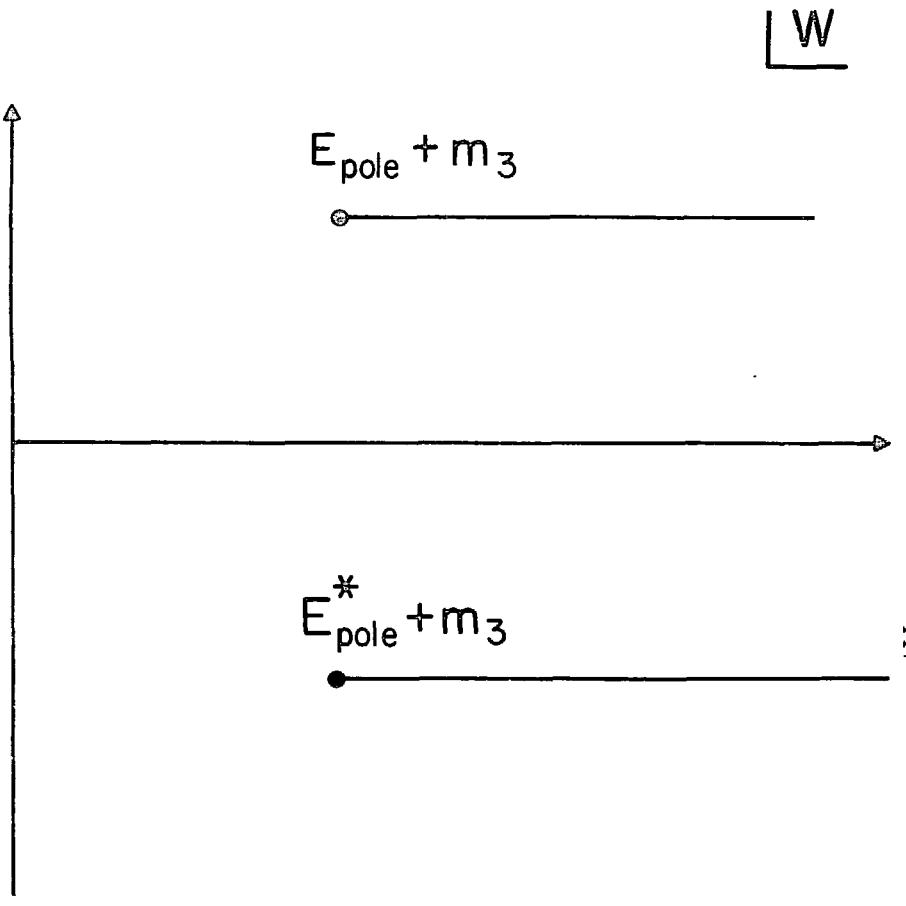

XBL7311-4469

Fig. 7.

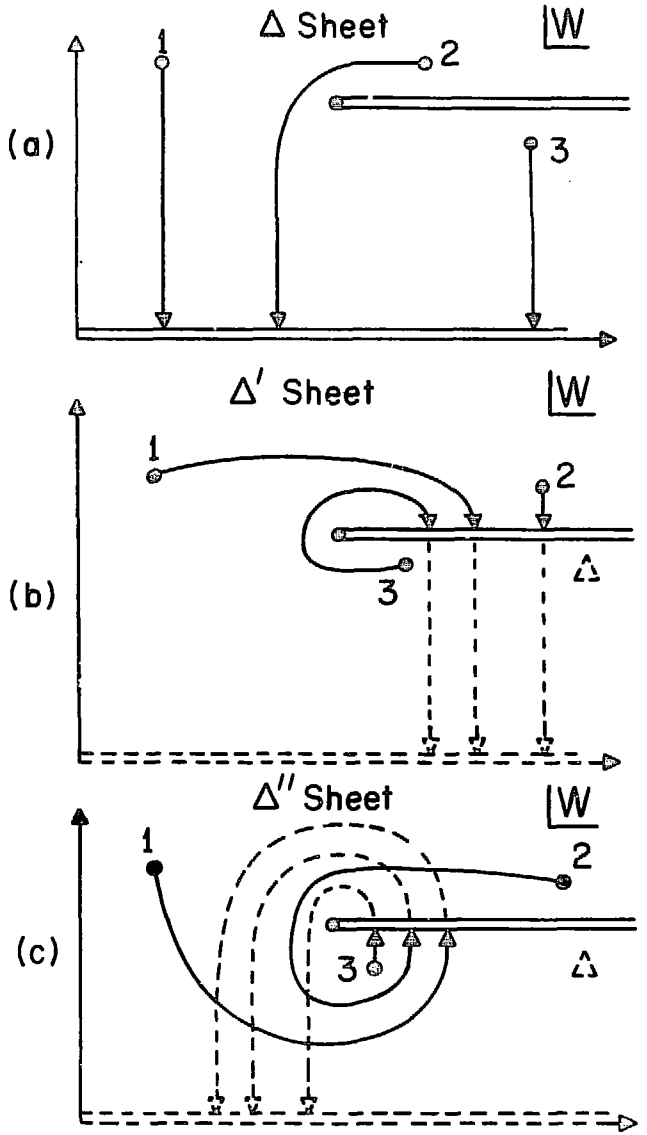

Fig. 9.

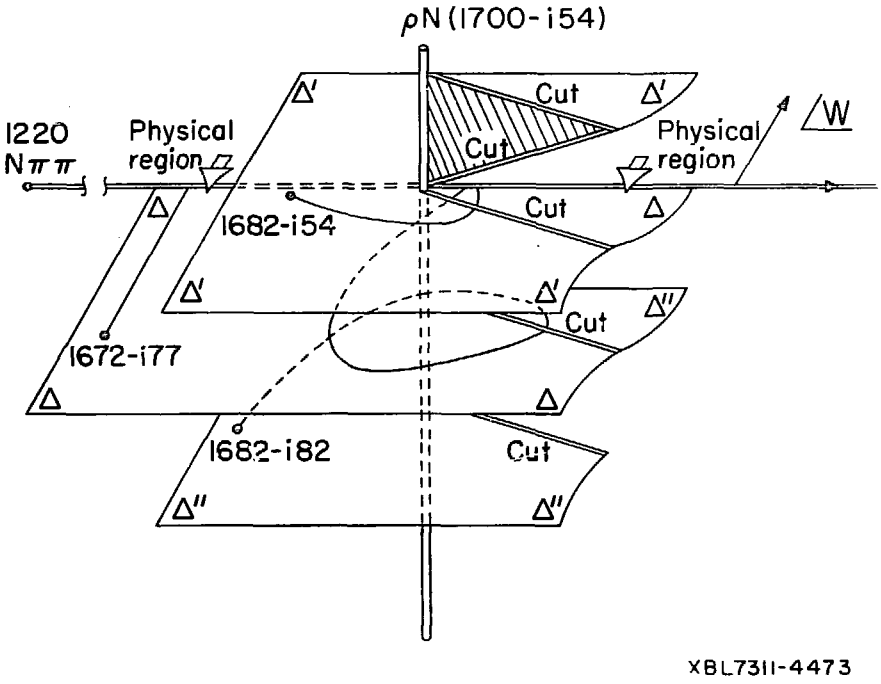
ρN(1700-i54)
1220
Nππ
Physical
region
Physical
region
W
Cut
Cut
Cut
Cut
Cut
Δ'
Δ''
Δ
1682-i54
1672-i77
1682-i82
XBL7311-4473

Fig. 10.

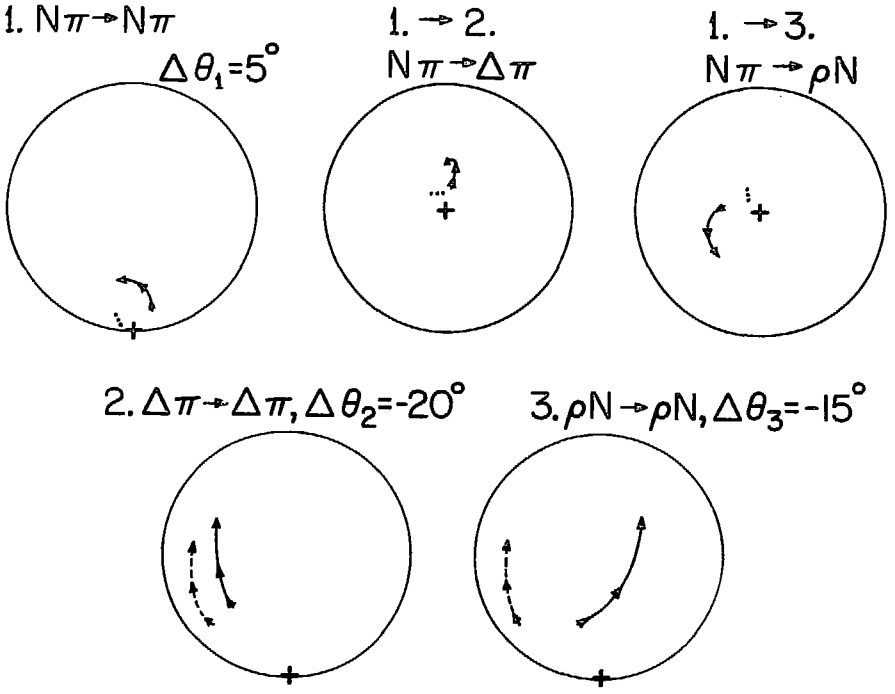

XBL7311-4472

Fig. 11.

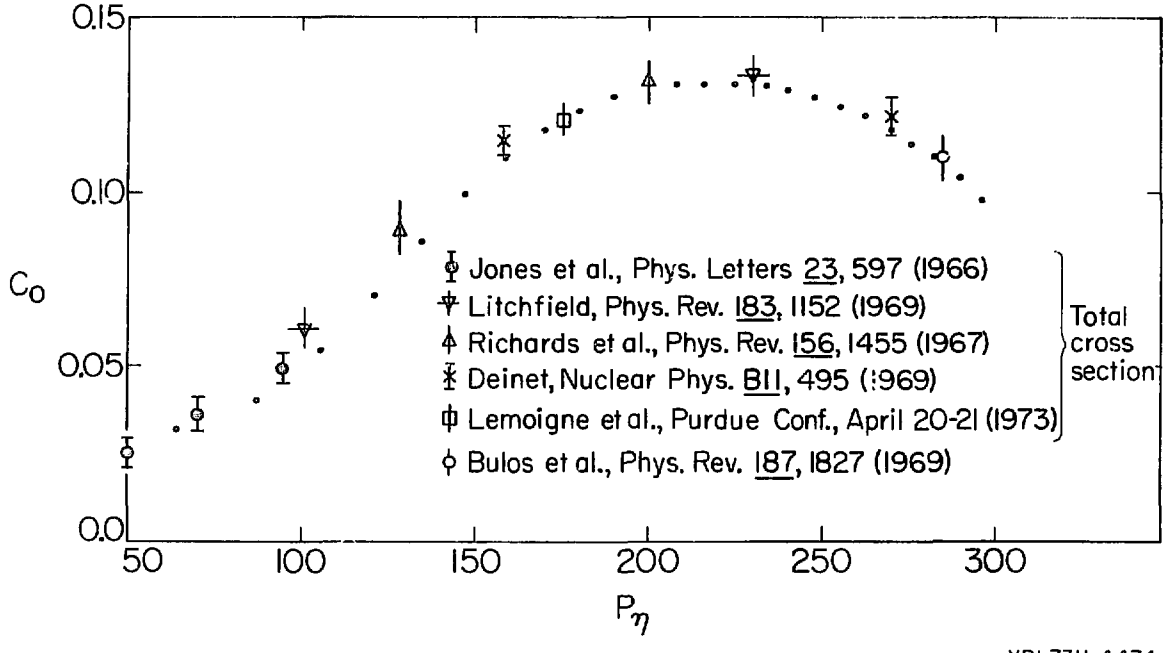
0.15
0.10
0.05
0.0
C_0
50
100
150
200
250
300
P_η
Jones et al., Phys. Letters 23, 597 (1966)
Litchfield, Phys. Rev. 183, 1152 (1969)
Richards et al., Phys. Rev. 156, 1455 (1967)
Deinet, Nuclear Phys. B11, 495 (1969)
Lemoigne et al., Purdue Conf., April 20-21 (1973)
Bulos et al., Phys. Rev. 187, 1827 (1969)
Total cross section
XBL7311-4474

Fig. 12.